NASA TECHNICAL NOTE

NASA TN D-4715

NASA TN D-4715

SOME OBSERVATIONS CONCERNING THE OXIDATION OF THE COBALT-BASE SUPERALLOY L-605 (HS-25)

by James S. Wolf and Gary D. Sandrock

Lewis Research Center
Cleveland, Ohio

NATIONAL AERONAUTICS AND SPACE ADMINISTRATION • WASHINGTON, D. C. • AUGUST 1968

NASA TN D-4715

SOME OBSERVATIONS CONCERNING THE OXIDATION OF THE COBALT-BASE SUPERALLOY L-605 (HS-25)

By James S. Wolf and Gary D. Sandrock

Lewis Research Center
Cleveland, Ohio

NATIONAL AERONAUTICS AND SPACE ADMINISTRATION

For sale by the Clearinghouse for Federal Scientific and Technical Information
Springfield, Virginia 22151 – CFSTI price $3.00

ABSTRACT

The concentration of the minor alloying elements silicon and manganese were found to strongly affect the oxidation behavior of L-605 in the temperature range 1000° to 1200° C. Silicon is also dominant in determining the post-aging ductility of this alloy. Plots were developed which indicate that it is possible to optimize both oxidation resistance and ductility of L-605 by restricting the silicon and manganese concentrations to the range 0.1 to 0.4 and 1.4 to 1.65 weight percent, respectively. A mechanism compatible with observed weight gains, scale structures, and scale compositions was proposed for the oxidation of L-605 and similar alloys.

SOME OBSERVATIONS CONCERNING THE OXIDATION OF THE COBALT-BASE SUPERALLOY L-605 (HS-25)

by James S. Wolf and Gary D. Sandrock

Lewis Research Center

SUMMARY

The concentration of the minor alloying elements silicon and manganese strongly affects the oxidation behavior of L-605 in the temperature range 1000° to 1200° C. Silicon is also dominant in determining the post-aging ductility of this alloy. Plots were developed which indicate that it is possible to optimize both oxidation resistance and ductility of L-605 by restricting silicon and manganese concentrations to the range 0.1 to 0.4 and 1.4 to 1.65 weight percent, respectively.

Good oxidation resistance within this compositional range is characterized by a smooth, nearly parabolic scaling process and results in the formation of scales composed essentially of chromium oxide and a spinel phase. Poor oxidation resistance, for alloys outside the suggested range of composition, is characterized by sudden increases in weight, the incidence of which is not predictable. The magnitude of these increments increases as the time to their initiation is increased. This anomalous phenomena is especially associated with alloy heats relatively low in both silicon and manganese concentration and is accompanied by the formation of additional scale layers of cobaltous tungstate and a spinel which form near the alloy-oxide interface.

A mechanism compatible with these observations is proposed for the oxidation of L-605. It is further postulated that this mechanism may be extended to rationalize the anomalous oxidation behavior of that large class of alloys on which highly stressed scales form.

INTRODUCTION

Load bearing members of air breathing engines or other devices subject to high-temperature corrosion should be designed to withstand failure by both stress and oxidation. It is also desirable that candidate materials possess sufficient ductility after ex-

posure at service temperature to resist failure by processes such as thermal cycling. One material that has found wide acceptance in the aerospace industry is the wrought cobalt-base superalloy L-605 (HS-25).

Though its strength properties, weldability, and fabricability are of sufficient quality to warrant its use, L-605 is subject to embrittlement in the temperature range 650° to 1100° C as are many other superalloys. The cause and methods of eliminating this embrittlement have been investigated (refs. 1 to 6). The cause has been associated with the precipitation of a Laves phase, situated mainly on grain and twin boundary sites of the matrix, which forms a nearly continuous network of brittle material. There are, at present, two principal methods for reducing this embrittlement: (1) the quantity of Laves phase has been reduced, and post-aging ductility increased, by lowering the silicon concentration of the alloy (refs. 3 to 5), (2) thermomechanical treatments have been found to redistribute the precipitate into a geometrical configuration which is less deleterious (refs. 5 and 6).

The effect of silicon concentration on post-aging ductility is shown in figure 1, which was adapted from the work of Nejedlik (ref. 5) and which includes the results of several other investigations as well as some NASA data not previously reported. Since it was found that the strength properties of L-605 were not grossly affected by reduction of the silicon concentration (ref. 4), it would appear desirable to both reduce the silicon concentration and apply thermomechanical techniques to its production (ref. 5), provided that

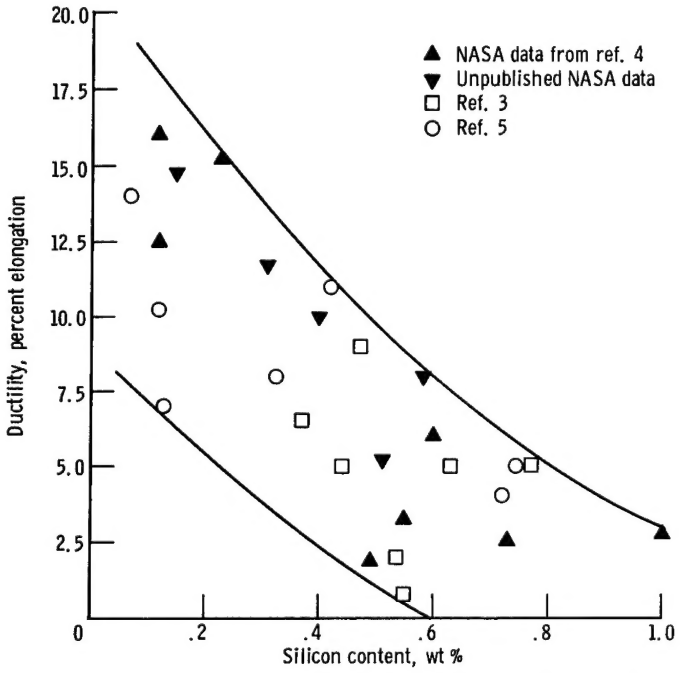

Figure 1. - Compilation of data showing effect of silicon concentration on ductility of L-605 aged 1000 hours at 871° C.

the reduction of silicon concentration does not lead to decreased oxidation resistance.

Although some research concerning the oxidation of L-605 has been performed (refs. 7 and 8), the effect of silicon concentration on the oxidation resistance of this alloy has received little attention. We have, therefore, undertaken a program to define the role of silicon concentration in the oxidation of L-605. Because the manganese and iron concentrations also varied in the heats investigated, their roles in the oxidation process were also studied. A series of alloys based on the nominal composition of L-605 but having silicon concentrations ranging from 0.12 to 1.00 weight percent, manganese concentrations ranging from 1.10 to 1.72 weight percent, and iron concentrations ranging from 0.57 to 3.24 weight percent were oxidized in air at temperatures between 1000° and 1200° C for times up to 225 hours. The degree and nature of the reaction was monitored by weight gain, metallographic, X-ray diffraction, and X-ray fluorescence techniques. An optimization of alloy composition as well as some insight into the mechanism of the oxidation process was evolved from these studies.

EXPERIMENTAL PROCEDURE

Materials Investigated

The nine commercially produced L-605 heats used in this investigation were re-

TABLE I. - COMPOSITION OF L-605 HEATS STUDIED

Heat	Analysis, wt %										ASTM average grain size
	Silicon[a]	Manganese	Iron	Chromium	Tungsten	Carbon	Nickel	Cobalt	Phosphorous	Sulphur	
1	0.23	1.52	0.57	20.02	15.02	0.13	10.40	Bal.	0.001	0.019	6
4	.55	1.52	1.60	20.07	14.62	.08	10.06		.012	.011	4
6	1.00	1.11	3.24	20.79	14.75	.10	10.14		.004	.011	6
8	.12	1.10	3.06	20.06	14.50	.12	10.27		-----	.005	6
A	.15	1.72	1.10	19.54	14.57	.08	10.02		.008	.011	4
B	.51	1.64	1.86	19.54	14.41	.09	10.61		.010	.010	3 to 4
C	.40	1.54	2.89	19.85	14.64	.07	9.91		.005	.006	4 to 5
D	.31	1.44	2.88	19.37	14.43	.15	10.00		.010	.019	7
E	.58	1.62	1.98	19.88	14.37	.08	10.31		.010	.010	4
AMS ranges	1 (max)	1 to 2	3 (max)	19 to 21	14 to 16	0.05 to 0.15	9 to 11	Bal.	0.04 (max)	0.03 (max)	-----

[a]Average of several determinations.

ceived in the form of hot-rolled and mill-annealed (1230° C solution treated; rapid air cooled) sheet material approximately a millimeter thick. All heats were analyzed by the vendors to determine their chemical compositions. In addition, determinations of the silicon concentrations were made by an independent laboratory. The results of these analyses, as well as the Aerospace Materials Specification (AMS) for composition ranges of L-605, are listed in table I. Note that each heat analysis is essentially within the ranges specified by AMS 5537B. All nine heats were used in the determination of post-aging ductility, but specimens from only seven heats (1, 4, 6, 8, A, B, and D) were used in oxidation tests.

Specimen Preparation

Fabrication. - The sheet material was cut into coupons each of which was approximately 2.5 centimeters long by 1.0 centimeter wide, providing specimens with a total surface area of approximately 5 square centimeters. In every case, the long dimension of the specimen was oriented parallel to the original rolling direction of the sheet material. Holes, approximately 2 millimeters in diameter, were punched or drilled through one end of each coupon so that it could be suspended by a platinum wire during oxidation.

Surface preparation. - The shaped specimens were surface ground using a rubber-bonded silicon carbide grinding wheel. Metal removal was limited to approximately 0.0005 centimeter per pass in order to minimize structural changes near the material surface. Specimens allocated for oxidation at 1100° and 1200° C received no further surface preparation, other than rinsing in reagent-grade ethanol, prior to oxidation. Specimens to be used for 1000° C oxidation experiments were provided with a 600-grit metallographic finish, rinsed in acetone, and finally rinsed in methanol prior to oxidation. All specimens were measured and their geomtric surface areas were calculated for use in normalization of weight-gain data.

Oxidation of Specimens

Oxidation at 1000° C. - Prepared specimens of L-605 were weighed to an accuracy of ±0.1 milligram and were subsequently emplaced in the fixture shown in figure 2. Each specimen was suspended by a platinum wire from a quartz rod which, in turn, rested on the upper lip of a Vycor container. The containers had small ports to allow a circulation of air about the entire specimen surface during oxidation. Seven containers, each holding one coupon of the seven heats investigated, were then placed on prebaked alumina bricks.

Six complete fixtures with specimens emplaced were oxidized simultaneously in a

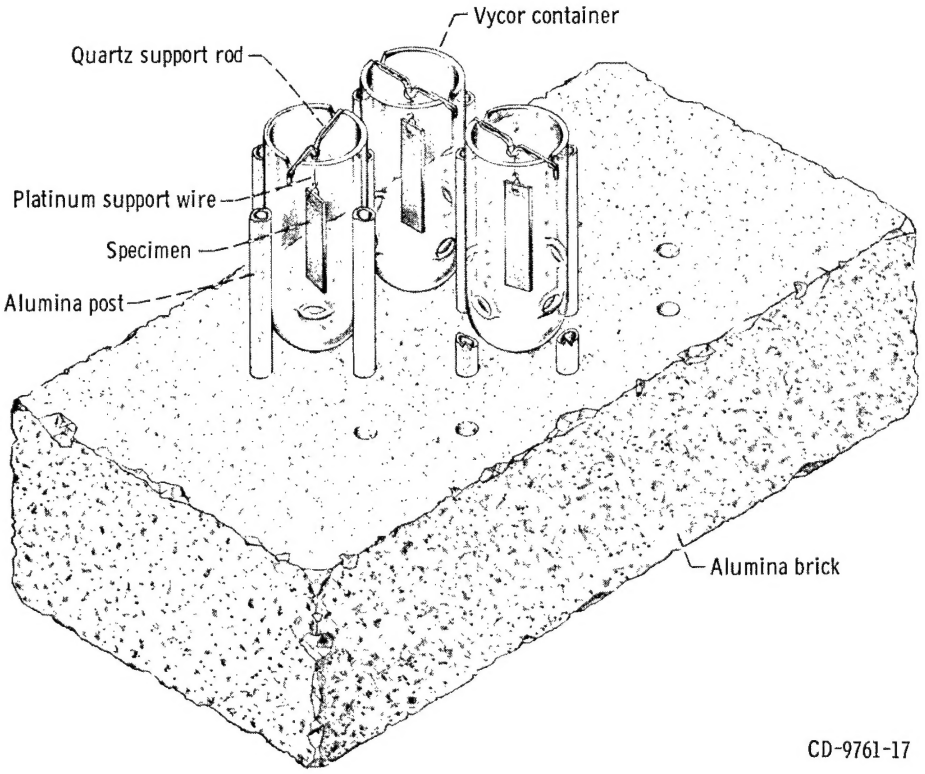

Figure 2. - Fixture for 1000° C oxidation tests.

large heat-treating furnace with an atmosphere of nominally static air. Two fixtures were removed from the furnace after 25, 100, and 225 hours, respectively. The furnace temperature was continuously recorded and was maintained at $1000^{\circ} \pm 10^{\circ}$ C. After removal from the furnace, the fixtures were covered by a sheet of clean stainless steel and allowed to cool to room temperature. Exfoliated material was thereby retained in the containers. The specimens, including their spalled products, were reweighed and the weight gain per unit area was calculated.

Oxidation at 1100° and 1200° C. - Because the maximum attainable temperature of the large heat-treating furnace was near 1000° C, oxidation tests at higher temperatures were performed using other equipment. Those experiments performed at 1100° and 1200° C utilized the continuous weighing apparatus shown in figure 3. Although it provided acceptable data at these temperatures, it was not sufficiently sensitive to be used at lower temperatures. Specimens, prepared as described previously, were suspended by a platinum wire from one pan of the automatic recording balance. With the furnace in its lowered position, a reference zero of weight was determined for the unoxidized specimen. The heated furnace was then raised to a position such that the specimen was contained within its center and a continuous weight-time record was begun. Analysis of this record provided data from which the weight gain per unit area was determined as a function of time.

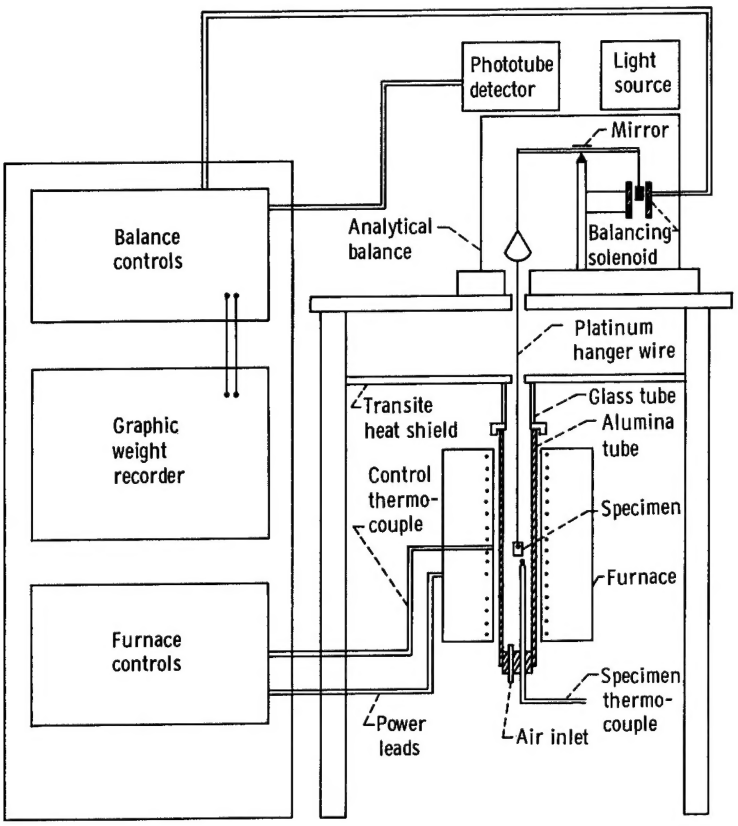

Figure 3. - Continuous weight-gain apparatus.

Aside from an initial temperature decrement of approximately 10° C which persisted for 2 to 5 minutes, the temperature was observed to vary less than $\pm 2^{\circ}$ C for the duration of these experiments. During oxidation air slowly flowed through the alumina furnace tube. After oxidation for preselected times, usually 4 or 100 hours, the furnace was lowered and the hanging specimen was allowed to cool to room temperature in place. In most instances a vial was placed around the cooling specimen so that spalled products could be retained for further analysis. Certain of those specimens oxidized for 100 hours at 1100° C were, however, not allowed to cool in place. They, with their scales in place, were quickly transferred to a mold into which a molten type-metal alloy was poured. The use of this technique allowed metallographic inspection of nearly complete scales.

Examination of Specimens

Metallographic examination. - The oxidized coupons mounted in type-metal alloy were immediately ready for metallographic preparation. Other specimens, subsequent to cooling and various inspections, were mounted either in Bakelite or a thermoplastic

mounting material. All specimens were positioned to show the oxide developed on their larger surfaces in cross section.

One or two millimeters were ground from the surface of each mount to avoid effects associated with specimen edges. Subsequently, standard techniques were employed to provide a metallographic polish of the sectioned coupon. Specimens were electrolytically etched in solutions composed either of (1) 30 cubic centimeters of saturated boric acid with 70 cubic centimeters of 10 percent sulfuric acid or (2) 30 cubic centimeters of 10 percent oxalic acid witn 15 cubic centimeters of concentrated sulfuric acid.

X-ray examination. - X-ray identification of oxide phases involved both powder camera and diffractometer techniques in which monochromatic chromium K_α and copper K_α radiation sources were employed. 114.6-Millimeter-diameter Debye-Scherrer cameras were used for powder analyses. Samples for these cameras were composed of ground, spalled products or scrapings from specimen surfaces. Cooled specimens, with their scales in place, were analyzed using a diffractometer outfitted with a horizontal goniometer. Identification of the crystalline phases present in the scales of oxidized alloys and assignment of their probable chemical constitution were made by comparing the experimentally determined diffraction patterns with established patterns of the ASTM Hanawalt X-ray index.

Most of the diffractometer determinations revealed that the incident beam penetrated the entire scale thickness, thereby providing a series of diffracted lines from the metallic substrate. When these lines were not observed, outer portions of the scale were mechanically removed by careful grit blasting with aluminum oxide, and a second pattern was determined. The second pattern always contained lines characteristic of the substrate. In every instance where the application of this technique was necessary, an inner-scale layer of cobaltous tungstate was found.

Selected specimens were analyzed using both X-ray diffraction and X-ray fluorescence techniques. The results of fluorescence analyses reinforced chemical identifications made by diffraction analyses. In addition, X-ray fluorescence was coupled with sequential aluminum oxide grit blasting of coupons to provide information concerning the sequence of occurrence of phases on oxidized specimens. Coupons with their scales thus totally removed were compared with unoxidized coupons from the same heat in order to gain information concerning the depletion or enrichment of metallic components of the alloy resulting from oxidation.

RESULTS AND DISCUSSION

Oxidation Data

Weight gain. - The weight gain data for all experiments are summarized in table II

TABLE II. - SUMMARY OF WEIGHT-GAIN AND X-RAY DATA

Heat	Time, hr	Final weight gain, mg/cm^2	Oxide phases identified[a]
Temperature, 1000° C			
1	25	0.56	C S3
	25	1.00	M S1
	100	.71	C S3
	100	.85	C S3
	225	1.08	
	225	1.10	
4	25	1.71	
	25	1.13	
	100	1.46	M C S1 W
	100	2.67	C S3
	225	1.30	
	225	.93	
6	25	0.39	C S3
	25	.80	C S3
	100	.80	C S3
	100	.81	C S3
	225	1.20	C S3
	225	1.46	
8	25	[b]3.36	M C S1 S3 T
	25	.66	C S3
	100	[b]8.93	M S1 T
	100	1.24	M C S3?[c]
	225	1.08	C S3?[c] W?[c]
	225	.99	M C S3?[c]
A	25	1.65	
	25	1.65	
	100	2.56	M C S1
	100	1.97	M C S1 S2
	225	2.10	
	225	2.12	
B	25	1.14	C S3
	25	1.57	C S3
	100	3.10	C S3
	100	1.05	M?[c] C S3
	225	1.16	C S2 S3
	225	1.30	C S3
D	25	0.90	
	25	.79	
	100	1.45	C S2
	100	.84	C S3
	225	1.15	
	225	.87	
Temperature, 1100° C			
1	4	0.46	M C S3
	40	2.21	
	100	2.24	
4	4	1.06	C S3
	4	.81	
	40	1.94	
	100	2.26	
6	4	1.17	C S3
	100	[b]6.57	
8	4	[d]3.00	M S1 T
	4	.93	M?[c] C S3
	66	[d]3.96	C S2 W
	100	[d]12.12	M C S1 T?[c]
	100	[d]8.12	
	101	5.15	
Temperature, 1200° C			
1	4	1.79	M S1
4	4	1.37	M C S1
6	4	1.51	M C S1
8	4.3	[e]4.85	M S1

[a]See table III for identification code.

[b]Suspected anomalous weight increments.

[c]Positive identification not possible.

[d]Documented anomalous weight increments.

[e]"Superlinear" oxidation behavior.

and representative portions of it are shown graphically in figures 4 to 6. There are certain aspects of the weight-gain curves which appear to be common to all temperatures of investigation: (1) oxidation tends to be parabolic in character, (2) anomalous weight increments may occur during oxidation, and (3) there is a marked dependence of the weight gain on the concentration of the minor alloying elements silicon and manganese. Effects (2) and (3) will be discussed at length in other sections of this report.

Figure 4 shows the weight increase, averaged for two specimens, incurred by seven different heats of L-605 during oxidation in air at 1000° C. The irregular appearance of the weight-gain - time curves is probably due to both material evaporation and specimen-to-specimen variation. Evaporation of the alloying constituents chromium and tungsten was indicated by fluorescent analysis of deposits on the glass tube of the apparatus shown in figure 3. Large specimen-to-specimen variations in weight gain are to be expected because anomalous weight increments may occur during oxidation.

The weight-gain curves for the seven individual heats, oxidized at 1000° C, tend to group into three distinct bands (fig. 4). The low-silicon, low-manganese concentration heat (0.12 wt % Si, 1.10 wt % Mn) has the least oxidation resistance. Alloys containing relatively little silicon (0.23 and 0.31 wt %) and intermediate amounts of manganese (1.44 and 1.52 wt %) or the alloy containing a high silicon concentration (1.00 wt %) with relatively little manganese (1.11 wt %) exhibit the best oxidation resistance. Variations

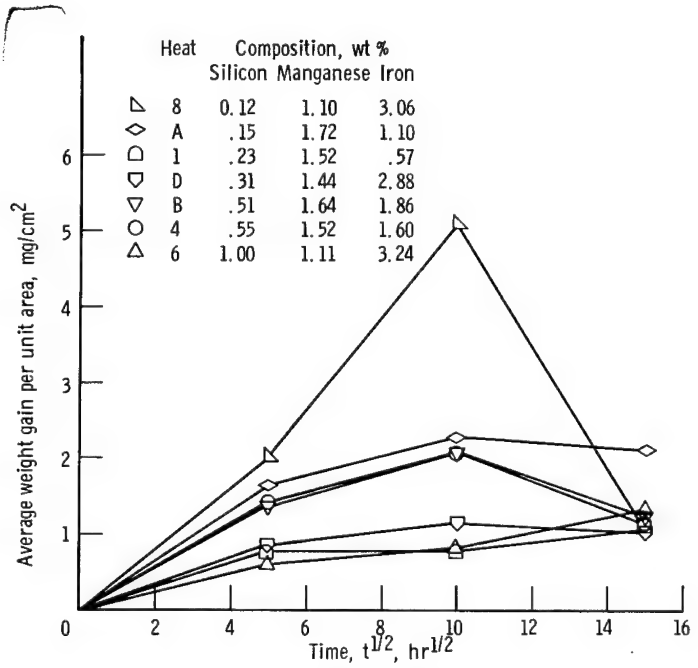

Figure 4. - Average weight gain per unit area as function of time for L-605 specimens from various heats oxidized in air at 1000° C. Note that curves group into three distinct bands which depend on combined concentrations of silicon and manganese.

in iron concentration appeared to have no consistent, detectable effect on the observed oxidation behavior of these alloy heats.

Typical results from 100-hour air oxidation tests at 1100° C are shown for specimens of four heats in figure 5. The continuous weight-gain technique employed in these tests provided positive evidence that anomalous, sharp weight increments occur during oxidation. The shapes of these curves also indicate that, in at least its terminal behavior, the scaling process tends to be approximately parabolic in character.

As in the case of the 1000° C oxidation experiments, the least resistant alloy at 1100° C contains low concentrations of both silicon and manganese (0.12 wt % Si, 1.10 wt % Mn). This is borne out by comparison of the magnitudes of both the terminal weight gains and terminal rates (slopes) (see fig. 5). The most oxidation resistant alloys contained intermediate concentrations of silicon (0.23 and 0.55 wt %) and, an intermediate concentration of manganese (1.52 wt %).

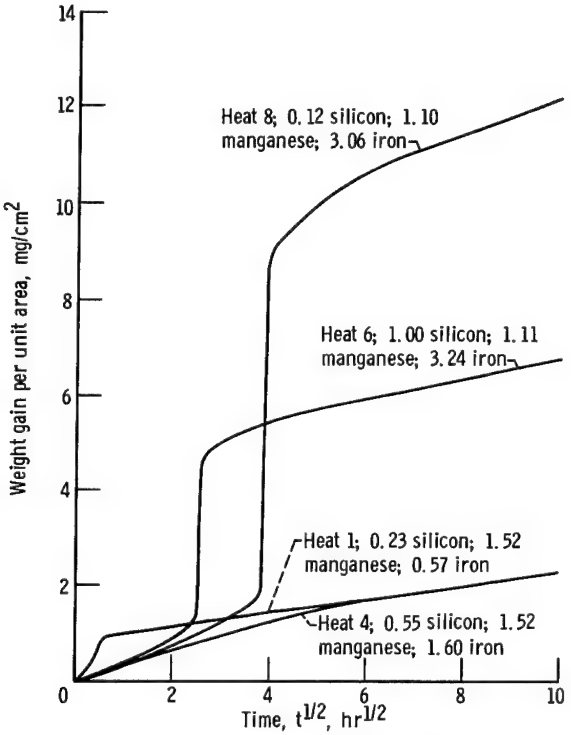

Figure 5. - Weight gain per unit area determined as continuous function of time for L-605 specimens from various heats oxidized in air at 1100° C. Note anomalous sharp weight increment characteristic of certain of these heats. (Alloy compositions are given in wt %.)

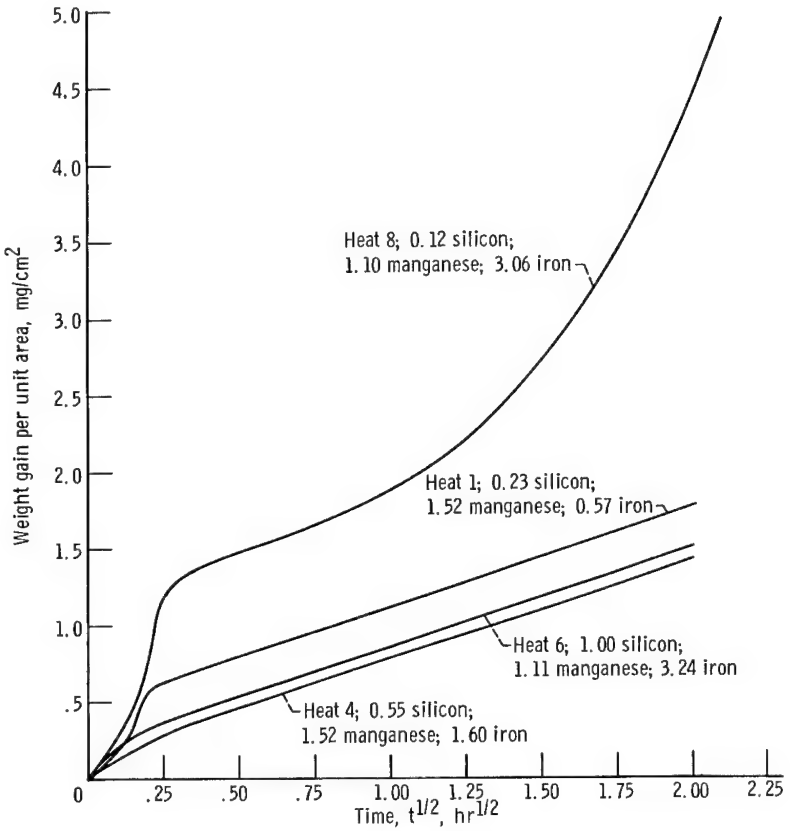

Figure 6. - Weight gain per unit area determined as continuous function of time for L-605 specimens from various heats oxidized in air at 1200° C. Note accelerated oxidation of specimen containing 0.12-weight-percent silicon and 1.10-weight-percent manganese. (Alloy compositions are given in wt %.)

Continuous weight-gain curves of specimens from four heats of L-605, oxidized in air at 1200° C, are shown in figure 6. The scaling process is again essentially parabolic for alloys containing 0.23 weight-percent silicon or more. Parallel with the findings at lower temperatures, the 0.12-weight-percent silicon - 1.10-weight-percent manganese heat exhibits the poorest oxidation resistance. Because the weight gain for this specimen increased at a faster than linear rate, the terminal oxidation process was termed "super-linear." As in the case of the 1000° C tests, variations in iron concentration appeared to have no consistent, detectable effect on oxidation behavior.

Weight-gain data from this investigation as well as data of references 7 and 8 are summarized and compared in figure 7. Alloy composition and test temperatures involved differ slightly as noted on the figure. The curves on this graph represent continuous weight-gain measurements, whereas the single data points shown are average values determined from two tests at 1000° C, which were not continuously monitored. Taken as a whole, the data tend to obey parabolic kinetics (slope = 1/2). Agreement between differ-

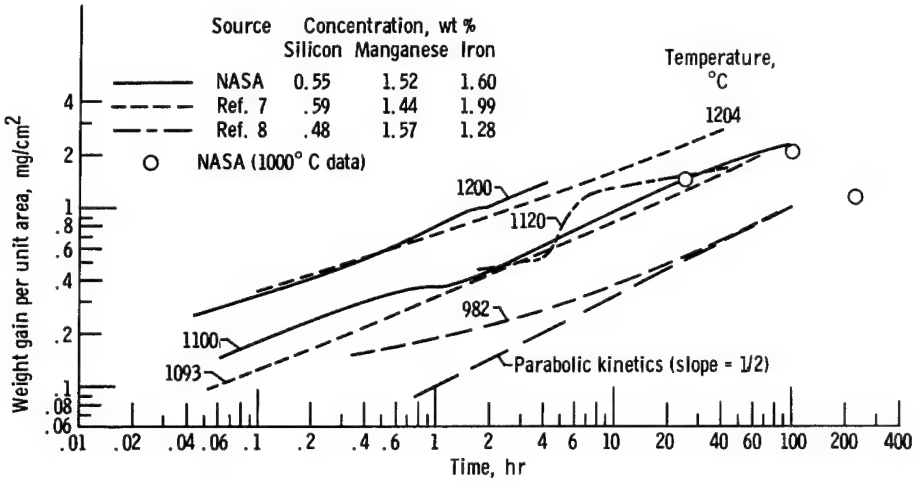

Figure 7. - Comparison of weight-gain data from this and other investigations for L-605 heats of intermediate silicon and manganese concentrations. Oxidation temperatures, 982° to 1204° C.

ent investigations is considered fair to good in view of the many possible differences in experimental procedures involved.

Oxide phases detected. - Phase analyses were made by X-ray diffraction, with only minor amounts of supplementary information from X-ray fluorescence and metallographic analysis; thus, the structural character, but not the precise chemistry, of the phases was determined. For example, the cubic phase identified as cobaltous oxide may in reality be a cubic solid solution of cobalt, nickel, iron, and manganese oxides with cobalt being the dominant metallic component. A complete listing of the phases identified in oxidized L-605 and their nominal compositions is given in table III.

The oxide phases present after completion of the scaling reaction are listed for each

TABLE III. - PHASES IDENTIFIED IN SCALES OF OXIDIZED L-605

Phase	Nominal formula	Symbol	Lattice parameter, Å (10^{-10} m)
Cobalt monoxide	CoO	M	4.25
Chromium oxide	Cr_2O_3	C	N.D.[b]
Spinel	$CoO \cdot Cr_2O_3$	S1	8.15 to 8.29
Spinel	?[a]	S2	8.30 to 8.40
Spinel	$MnO \cdot Cr_2O_3$?[a]	S3	8.41 to 8.55
Cobaltous tungstate	$CoWO_4$	T	N.D.[b]
Tungsten metal	W	W	4.84

[a]Uncertain.
[b]Not determined.

specimen in table II. In addition to the oxides, a limited number of scales contained metallic tungsten which is also listed. Lack of any entry in this table indicates that X-ray diffraction patterns were not obtained for the specimen in question.

The data concerning phases identified in scales of oxidized coupons exhibited trends dependent essentially on oxidation temperature and alloy composition. Low oxidation temperatures favor the formation of chromia in combination with a spinel of large lattice parameter (~8.5 Å or 8.5×10^{-10} m) which, therefore, is probably rich in manganese. This combination of phases was usually present in specimens of relatively low weight gain at 1000° C. At the highest temperature, the dominant phases are cobalt monoxide and a spinel of low-lattice parameter, which is probably deficient in manganese. Low concentrations of both silicon and manganese (0.12 wt % Si, 1.10 wt % Mn) lead to the formation of cobaltous tungstate, a phase found exclusively in scales formed on this alloy heat. The presence of the tungstate phase correlated with those specimens that exhibited inordinately large weight gains. A further discussion of the roles of silicon and manganese concentrations on the existence of oxide phases will be presented later.

Metallography of oxidized specimens. - The reaction products formed during the oxidation of L-605 were found in two major zones: one on the surface as a nominally continuous scale and the other within the metal as a region of subsurface particles or subscale. Furthermore, the surface scale was usually constituted of several layers, each having a unique set of physical and chemical characteristics. Photomicrographs of typical scales, formed at each of the temperatures investigated, are shown in cross section in figures 8 to 10. In each of these figures mounting material is shown on the left edge of each photomicrograph and unaffected alloy is at the right edge.

Figure 8 shows the structural character of the scaled alloy heats after oxidation for 100 hours at 1000° C. The external scale is complete only in figure 8(a) which shows that at least two and perhaps three layers are present in the external scale. The outermost layer is cobalt monoxide and underlying it are the spinel(s) and chromia. Beneath the apparent alloy-oxide interface of each oxidized coupon lie the subscale oxide particles in a zone otherwise depleted of the more reactive alloying elements. The subsurface oxides penetrate the alloy most deeply in regions previously occupied by the Laves phase which is present especially at grain and twin boundaries of the alloy. This phase appears to increase in volume concentration as the silicon content of L-605 is increased (fig. 8 and ref. 4). In turn, the subscale particles, although discrete at low silicon concentrations, are more numerous, have smaller interparticle spacings, and tend to become a continuous oxide network at high silicon concentrations.

Microstructures of sectioned specimens oxidized for 100 hours at 1100° C are illustrated in figure 9. Because these specimens were cast into type metal on cooling, the external scales are essentially complete and reflect the degree of their formation. Coupons that exhibited anomalous, large weight increments have thick scales containing sev-

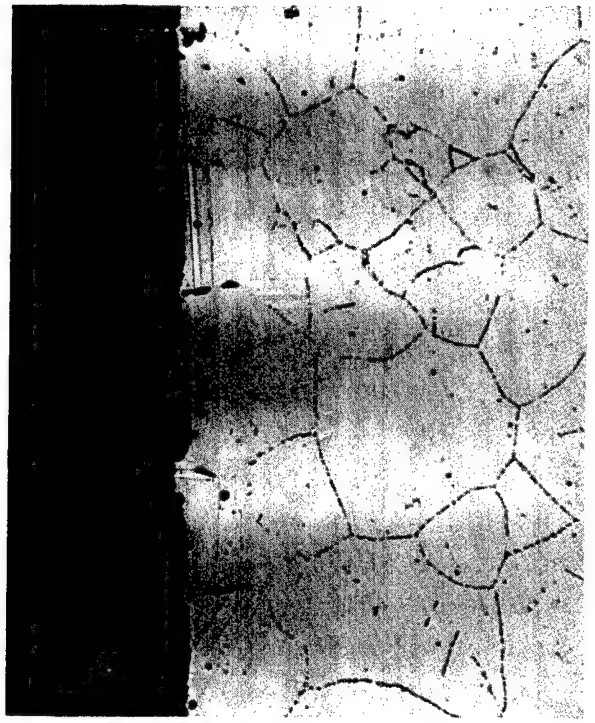

(a) 0.15-weight-percent silicon; 1.72-weight-percent manganese.

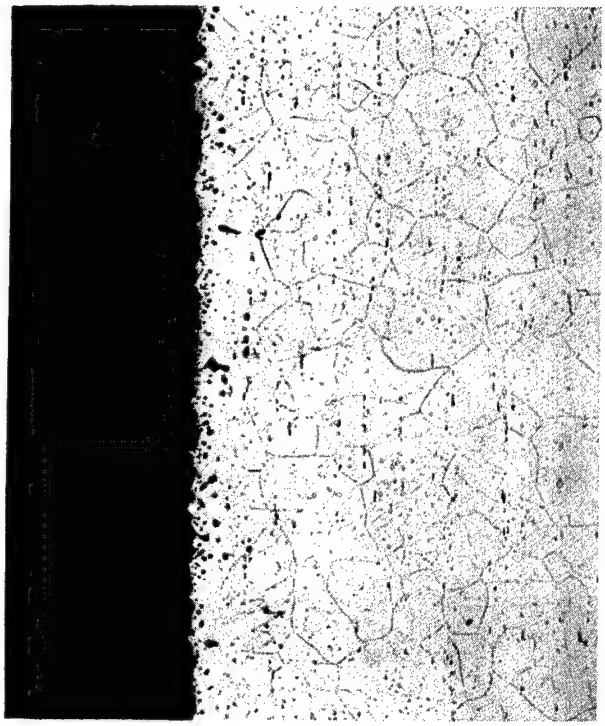

(b) 0.23-weight-percent silicon; 1.52-weight-percent manganese.

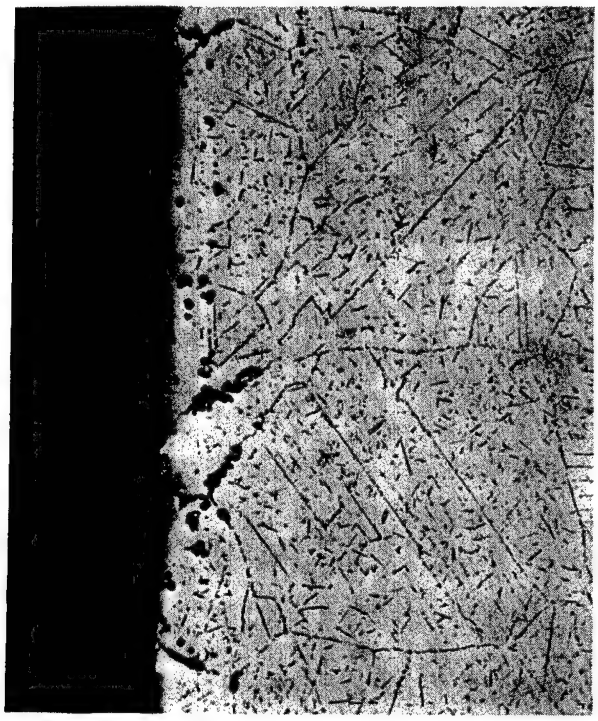

(c) 0.55-weight-percent silicon; 1.52-weight-percent manganese.

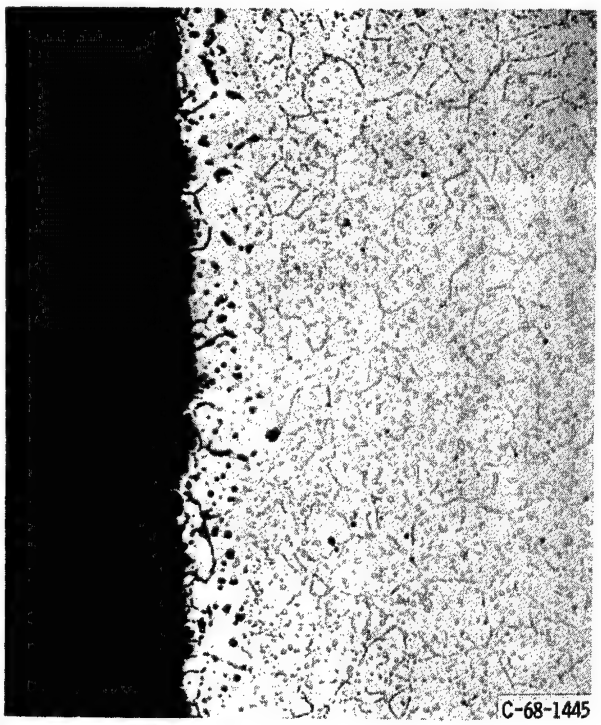

(d) 1.00-weight-percent silicon; 1.11-weight-percent manganese.

Figure 8. - Cross sections of L-605 specimens from various heats oxidized for 100 hours in air at 1000° C. Note variation in distribution of subscale oxide particles with silicon concentration. Etched with sulfuric acid - boric acid mixture. X250.

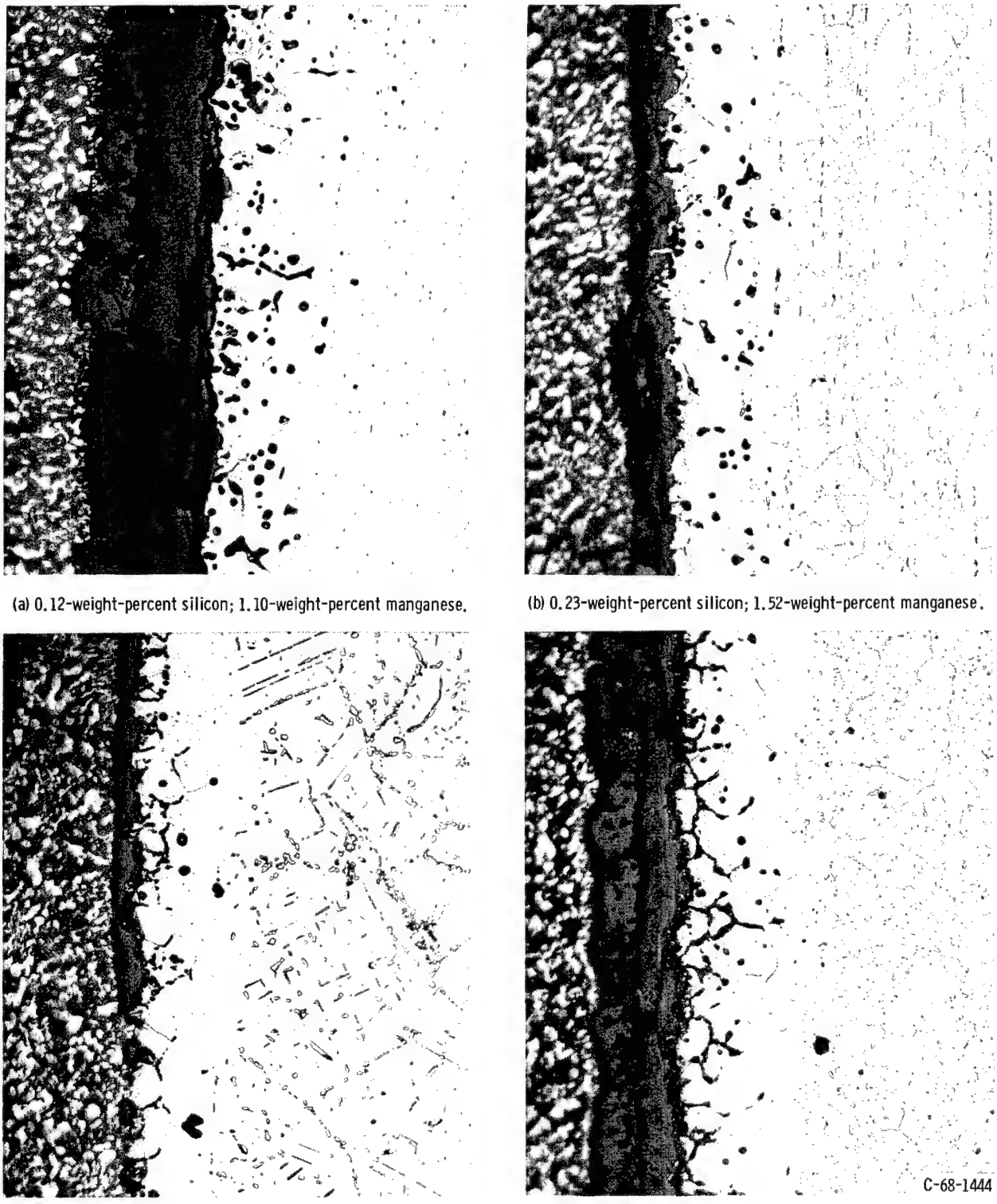

(a) 0.12-weight-percent silicon; 1.10-weight-percent manganese.

(b) 0.23-weight-percent silicon; 1.52-weight-percent manganese.

(c) 0.55-weight-percent silicon; 1.52-weight-percent manganese.

(d) 1.00-weight-percent silicon; 1.11 weight-percent manganese.

Figure 9. - Cross sections of L-605 specimens from various heats oxidized for 100 hours in air at 1100° C. The two specimens with thicker scales have undergone sharp weight increments. Etched with sulfuric acid - boric acid mixture. X250.

eral layers (figs. 9(a) and (d)), but those that exhibited smooth oxidation curves had thinner, simpler scale structures. As in the case of specimens oxidized at 1000° C, the continuity of the Laves phase, and subsequently that of the subscale particles, increases with increasing silicon concentration. Depletion zones are, in this case, wider, and the Laves phase has precipitated as coarser particles with larger interparticle spacings. At 1100° C no Laves phase was observed metallographically in the tested 0.12-weight-percent silicon specimen.

The microstructures of specimens oxidized for 4 hours at 1200° C (fig. 10) vary markedly from those produced at lower temperatures in that the Laves phase is essentially absent. This observation is in agreement with previously reported data (ref. 3). Some Laves phase, in spheroidized form, is present in the heat of highest silicon concentration (see fig. 10(d)). Particles of the internal oxide selectively form at alloy grain boundaries, suggesting that the boundaries contain high concentrations of Laves phase constituents though they do not precipitate as the intermetallic. As at lower temperatures, this subscale distribution is more prevalent and tends to be more interconnected for heats containing larger silicon concentrations.

A unique type of localized attack was noted for the heat containing low concentrations of both silicon and manganese (see fig. 10(a)). The external scale in this case is comprised in part of large nodules which entrap numerous metallic particles near the metal-oxide interface. The presence of this structural feature correlates with the superlinear oxidation noted earlier.

The Laves phase, nominally a cobalt-tungsten (Co_2W) intermetallic in this alloy, is stabilized by the presence of silicon (refs. 3 and 4). Silicon also stabilizes this phase in several other alloys having similar electron-to-atom ratios (ref. 9). This silicon effect is suggested by the photomicrographs of figures 8 and 9. Certain investigators have found evidence suggesting that this phase may contain as much as 1/6th silicon, corresponding to the composition $(Co_3Si)\ W_2$ (ref. 9). In this case, the silicon substitutes for a fraction of the cobalt atoms in Co_2W. Preferred oxidation of this phase, noted earlier, should lead to internal oxide particles rich in silicon. One investigator has, indeed, observed that silica is associated with the subscale zone (ref. 7); however, that result was not substantiated in the course of this research. X-ray examination of particles mechanically removed from the subscale region of a 1.00-weight-percent-silicon - 1.10-weight-percent-manganese alloy after oxidation for 100 hours at 1000° C indicated the presence of a tungstate phase and some extra diffraction lines, which may or may not be associated with a silicon-bearing oxide. Intensity data indicated that the tungsten-containing phase was most probably nickelous tungstate; however, the possibility of mixed tungstates is not excluded.

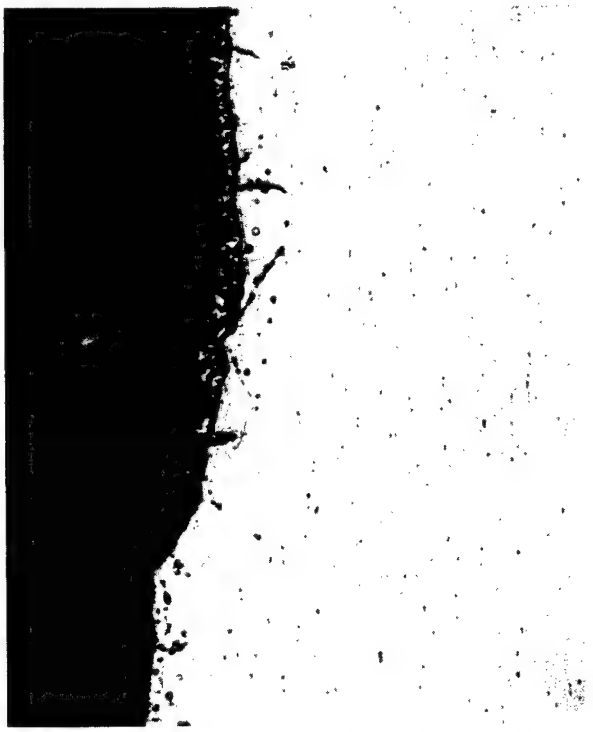

(a) 0.12-weight-percent silicon; 1.10-weight-percent manganese.

(b) 0.23-weight-percent silicon; 1.52-weight-percent manganese.

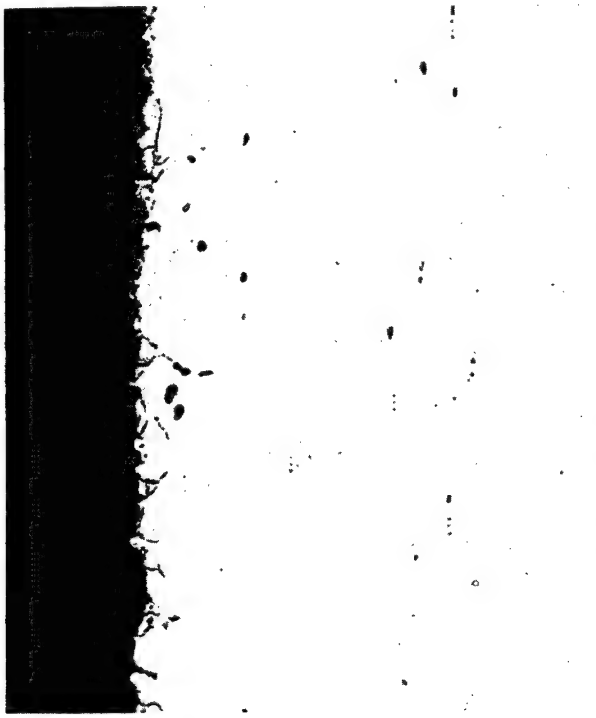

(c) 0.55-weight-percent silicon; 1.52-weight-percent manganese.

(d) 1.00-weight-percent silicon; 1.11-weight-percent manganese

Figure 10. - Cross sections of L-605 specimens from various heats oxidized for approximately 4 hours in air at 1200° C. Specimen with 1.00-weight-percent silicon exhibits spheroidized Laves phase particles in alloy matrix. Etched with sulfuric acid - oxalic acid mixture. X250.

Compositional Optimization of L-605

Both weight-gain and oxide phase existence data could be correlated by a plotting technique using as parameters the silicon and manganese concentrations. These correlations, presented graphically in figures 11 to 13, suggest that silicon and manganese act in concert to dictate both the type and degree of scale formation and that iron appears to play no major role in these processes. Note that the total area of each graph represents possible concentration limits of these elements as dictated by the Aerospace Materials Specifications (AMS).

Figure 11 shows the results of weight gain measurements and X-ray diffraction analyses obtained from coupons of seven heats oxidized at 1000° C. Iron concentrations, in weight percent, are shown in parentheses to the right of each compositional point on the silicon-manganese diagrams. The diagram of figure 11(a) is divided into four regions (bands) based on weight-gain data. The data of each specimen is ranked relative to that for all other specimens tested under the same conditions. Low weight gains were rated "good," intermediate weight gains were rated "fair," and mixed high and low weight gains were rated "unstable." These terms qualitatively describe the oxidation resistance of the alloys in question, the term "unstable" being especially applicable to those specimens that exhibited large weight increments. Although none of the alloy heat compositions fall into the bottom "fair" band, it was so labeled both intuitively and in accordance with data obtained at higher temperatures. The three occupied bands of figure 11(a) correspond to the banding of data noted in figure 4.

An identical division of the compositional field is used in figure 11(b), which shows that good oxidation resistance is accompanied by the formation of chromia and a high lattice parameter (probably manganese-bearing) spinel. Some specimens having fair oxidation resistance exhibited, in addition to these phases, cobalt monoxide and the spinel phases of lower lattice parameter. Free tungsten was detected in the scale of one alloy heat within this band. In the unstable band, the low weight-gain specimen had scales similar to those found in the good or fair regions, while, in contrast, the high weight-gain specimen exhibited cobalt monoxide and the low-lattice-parameter spinel in association with cobaltous tungstate. The tungstate phase was detected only in this unstable region.

At higher temperatures, the same type or correlation may be applied if the bands are broadened as shown in figures 12 and 13 for oxidation at 1100° and 1200° C, respectively. Using the same weight-gain criteria, only the unstable and bottom fair band (previously unoccupied) now appear.

Specimens oxidized at 1100° C in the composition region corresponding to fair oxidation resistance exhibit chromia and the high-lattice-parameter spinel in their scales. In one instance, cobalt monoxide is also present. Specimens oxidized in the composition region corresponding to the unstable band again exhibited duplex behavior. One of these

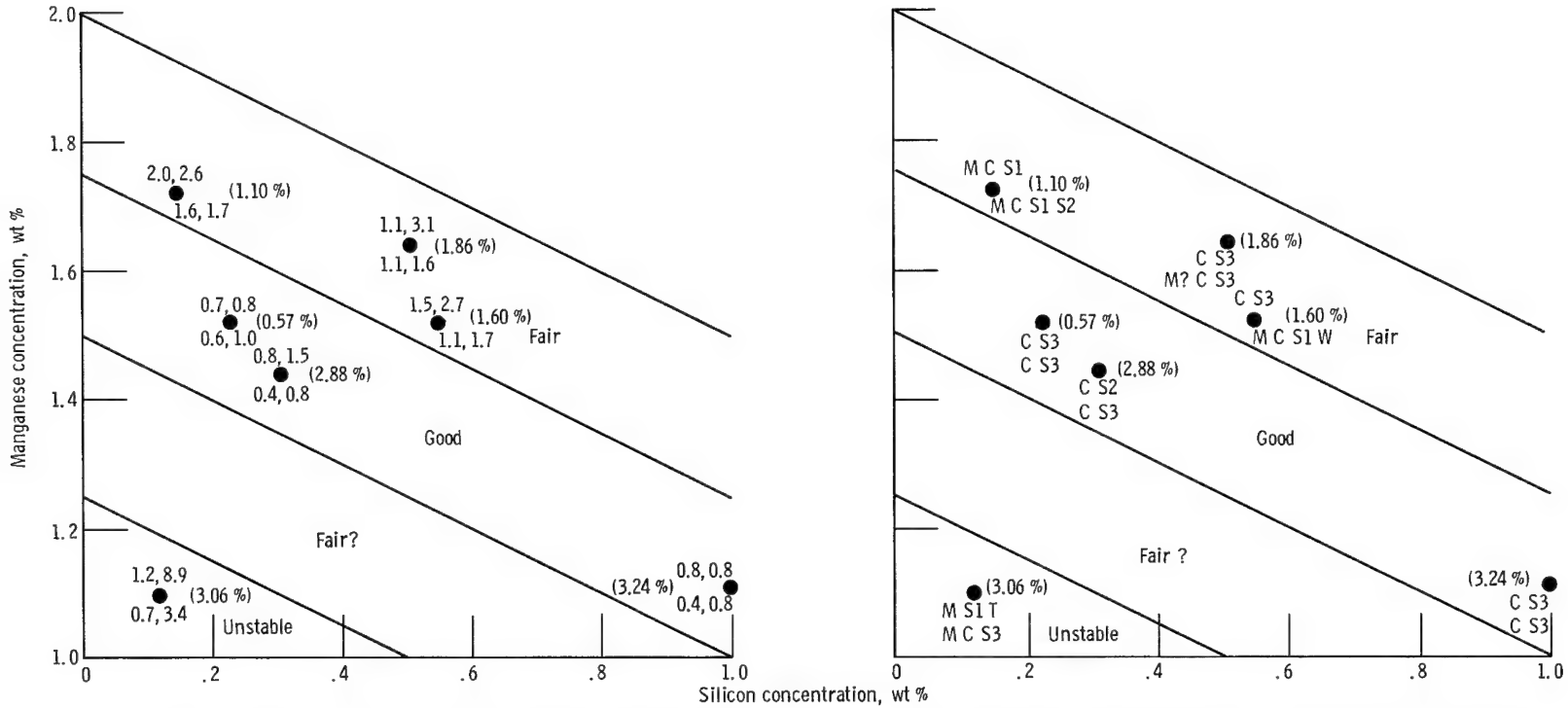

(a) Weight gain (mg/cm^2). Top numbers denote weight gains for 100 hours; bottom numbers denote weight gains for 25 hours.

(b) Oxide phases identified after 100 hours. (See table III for identification code.)

Figure 11. - Weight gain and oxide phases identified as function of silicon and manganese concentration for L-605 specimens oxidized in air at 1000° C. Note that specimens can be grouped on basis of both weight gain and phases identified. Iron concentrations for each compositional point are shown in parentheses.

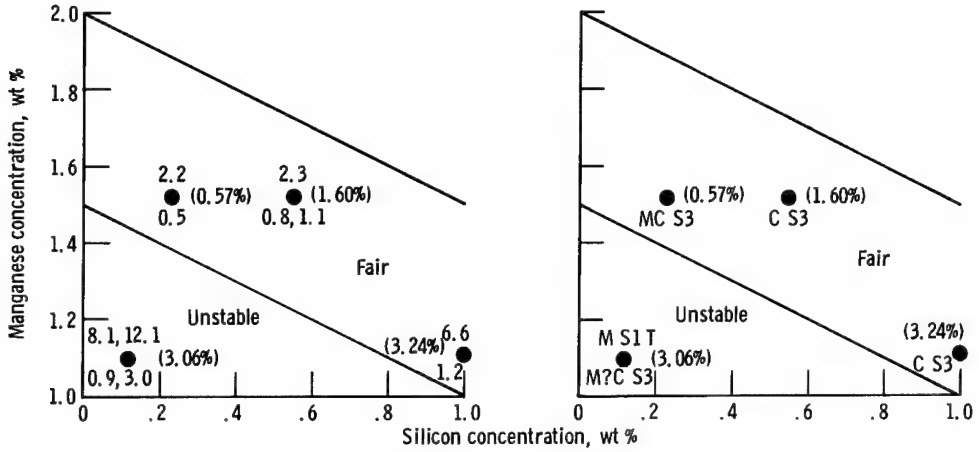

(a) Weight gain (mg/cm^2). Top numbers denote weight gains for 100 hours; bottom numbers denote weight gains for 4 hours.

(b) Oxide phases identified after 4 hours. (See table III for identification code.)

Figure 12. - Weight gain and oxide phases identified as function of silicon and manganese concentration for L-605 specimens oxidized in air at 1100° C. Note relatively high weight gains for specimens low in both silicon and manganese. Iron concentrations for each compositional point are shown in parentheses.

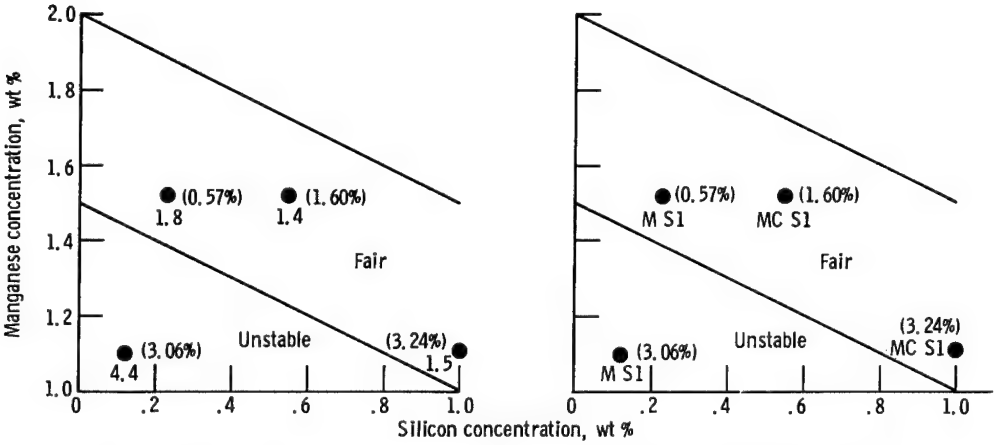

(a) Weight gain (mg/cm^2). Numbers denote weight gains for 4 hours.

(b) Oxide phases identified after 4 hours. (See table III for identification code.)

Figure 13. - Weight gain and oxide phases identified as function of silicon and manganese concentration for L-605 specimens oxidized in air at 1200° C. Consistent with data at 1000° and 1100° C, highest weight gain was observed on specimen with 0.12-weight-percent silicon and 1.10-weight-percent manganese. Iron concentrations for each compositional point are shown in parentheses.

specimens had characteristics of those in the fair band, the other showed large weight increments and had scales composed of cobalt monoxide, a low-lattice-parameter spinel, and cobaltous tungstate. This phenomenology is identical with that observed at 1000° C.

Data from specimens oxidized at 1200° C may be represented as was the 1100° C data. Specimens whose compositions lie in the fair band undergo parabolic scaling with low final weight gain, but the low-silicon, low-manganese concentration heat of the unstable region exhibits "superlinear" oxidation and a high final weight gain. The scales developed on coupons of all heats contained cobalt monoxide and the low lattice parameter spinel. The two heats of highest silicon concentration additionally exhibited chromia in their scales; however, this constituent did not appear to be the limiting factor with respect to the ranking of observed weight gains.

In figures 11 to 13, it may prove helpful to visualize the coordinate system employed as an analog to an isothermal section through an equilibrium phase diagram; the lines within the graphs being analogous to phase boundaries. These boundaries separate dissimilar bits of information into distinct regions, termed bands, which cut diagonally through the composition diagram. As temperature changes, the extent, but not the shape, of the bands is altered. This is analogous to the changes in isothermal sections through more conventional phase diagrams (e.g., ref. 10). This regime appears to apply in spite of the fact that the alloy-oxygen system never reaches a true equilibrium state.

However, it is interesting to note that the 1.00-weight-percent silicon heat (see fig. 12(a)), when oxidized for 100 hours at 1100° C, did show an unstable character. This behavior may indicate that the unstable region shifts upwards to include this composition as the system tends toward equilibrium at longer times.

From the information presented in figures 11 to 13, it is possible to choose a single composition range (or band) in which oxidation resistance is optimum for all temperatures of investigation. This band (fig. 14(a)) represents the good oxidation resistance compositions found at 1000° C and the better compositions (fair) found at higher temperatures. Similarly, an optimum composition range for post-aging ductility may be defined by plotting the NASA data of figure 1 in the same compositional coordinate system. In this case, elongations in excess of 10 percent were considered "good." This plot is shown in figure 14(b). Superposition of these two graphs defines a small common area on the composition diagram in which both oxidation resistance and post-aging ductility are good (see fig. 14(c)). Thus, it is determined that the heats having silicon concentrations ranging from approximately 0.1 to 0.4 weight percent and manganese concentrations ranging between approximately 1.4 and 1.65 weight percent possess both good post-aging ductility and good oxidation resistance.

These composition limits for silicon and manganese are within the AMS ranges of composition for L-605; however, commercial heats of this alloy can contain more silicon.

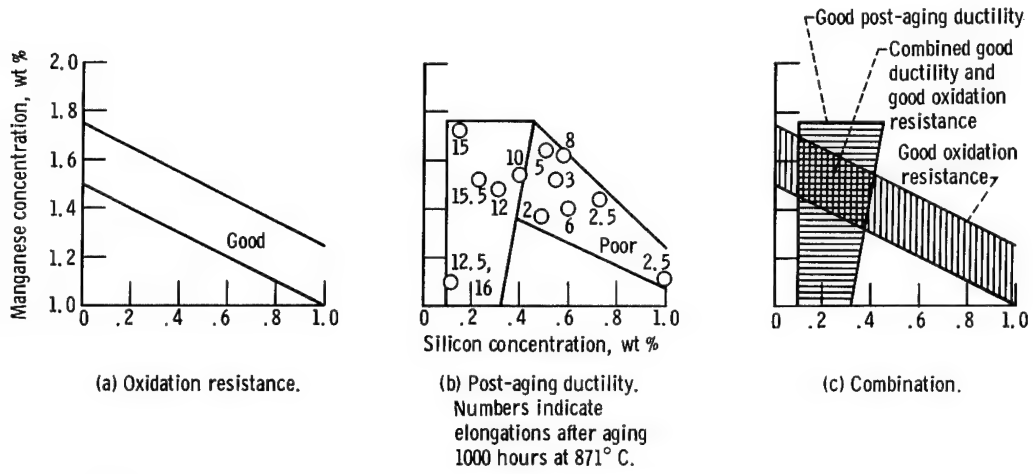

(a) Oxidation resistance.

(b) Post-aging ductility. Numbers indicate elongations after aging 1000 hours at 871° C.

(c) Combination.

Figure 14. - Combination of good oxidation resistance and good post-aging ductility as function of silicon and manganese concentration. Best combination of properties occurs in range of 0.1- to 0.4-weight-percent silicon and 1.4- to 1.65-weight-percent manganese.

On the basis of this research, we propose that, for high-temperature applications requiring superior oxidation resistance and ductility, the melting practice be altered and specifications written, such that the heats produced will fall within the narrower concentration limits just cited. This investigation provides no basis for alteration of Aerospace Materials Specifications concerning other alloying components of the L-605 superalloy.

Characterization of L-605 Oxidation

Anomalous weight increments. - One of the most striking aspects of this research, and one which provides information concerning the oxidation mechanism of L-605, is the observed occurrence of anomalous weight increments. The data concerning this feature of the oxidation process was evolved primarily during several independent continuous weight-gain tests of the low-silicon, low-manganese concentration heat at 1100° C where the total process is most evident. The concepts to be derived from these limited data are necessarily somewhat speculative in nature; however, they are believed to be generally applicable to this class of alloys.

Figure 15 illustrates the weight-gain - time relations observed for five continuous weight-gain experiments made under nominally identical conditions of temperature, alloy composition, and environment. The semilogarithmic plot is used here merely for convenience and is not meant to imply any mechanistic interpretation. In character, the weight gains increase smoothly along a single curve until some (unpredictable) time is reached after which they increase rapidly in an anomalous fashion. Subsequently, the

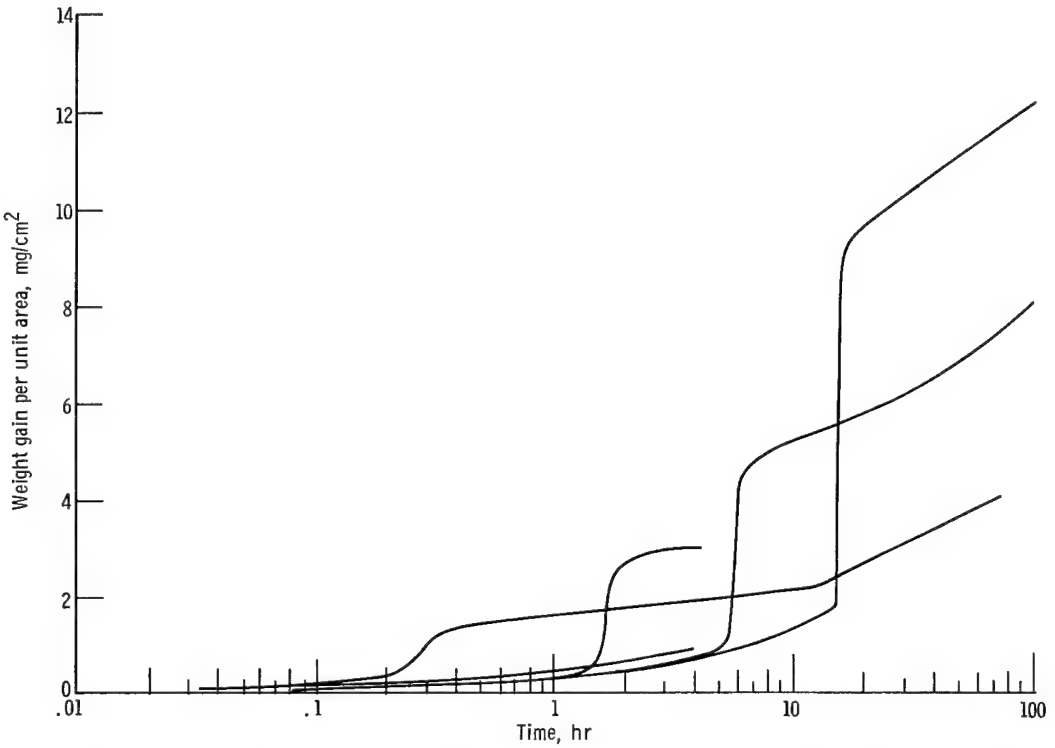

Figure 15. - Five oxidation runs in air at 1100° C for specimens from heat 8 (0.12 wt % Si, 1.10 wt % Mn). Note lack of reproducibility.

rate of weight increase diminishes. These limited data indicate that the probability of occurrence of an anomalous increment is approximately 50 percent in the first 4 hours of oxidation at 1100° C.

The amplitude of the anomalous weight increment increases linearly with increasing time as shown in figure 16. However, the weight gain prior to this increment increases in an approximately parabolic fashion with time (fig. 16) indicating that the reaction producing the anomalous increment is not merely a transformation due to further oxidation of pre-existing scale products. Analyses of curve shapes based on such a hypothesis were not fruitful, further reinforcing this argument.

If the weight-gain curve of figure 15 having the largest anomalous weight increment is replotted, it is seen that the initial and final phases of oxidation are parabolic and, furthermore, that approximately the same parabolic rate constant prevails before and after the anomalous increment (fig. 17). Because there is no necessity to shift the zero of time in order to regain later parabolic behavior, it is inferred that the protective nature of the scale formed prior to the anomalous increment is retained. The short-term, faster-than-parabolic rate immediately subsequent to the anomalous increment will be discussed in the section Proposed scaling mechanism.

In order to explore the causal relations of the anomalous weight increment, two no-

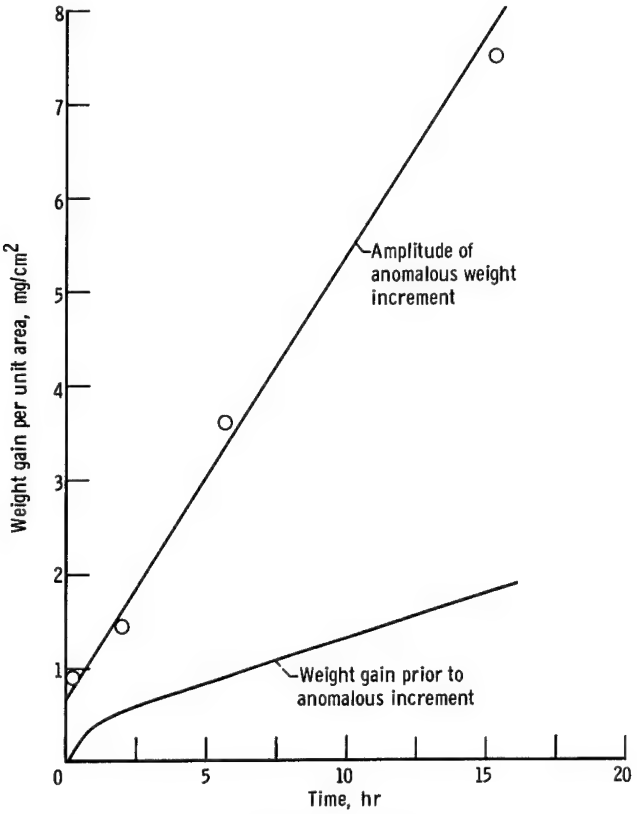

Figure 16. - Linear dependence of amplitude of anomalous weight increment on time to its initiation and nearly parabolic dependence of prior weight gain on oxidation time. (Data from curves of fig. 15.)

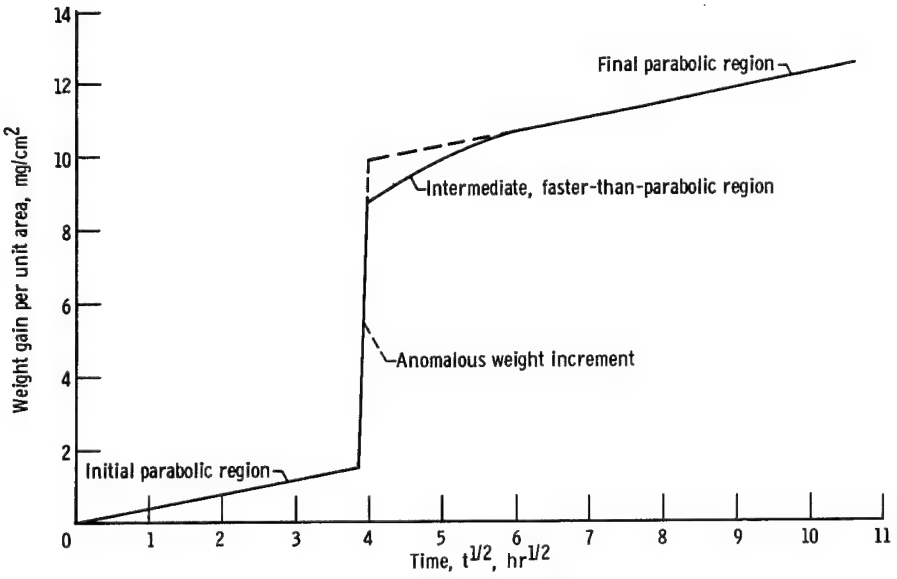

Figure 17. - Weight-gain curve for specimen of low-silicon, low-manganese heat of L-605, which exhibited largest anomalous weight increment at 1100° C. Note that initial and final parabolic rates (slopes) are nearly equal.

minally identical coupons were investigated in detail. Each specimen had been oxidized for 4 hours at 1100° C in air. One underwent smooth, parabolic scaling, but the other exhibited an anomalous weight increment (see fig. 15). Microstructural features of these specimens are shown in figure 18, wherein all photomicrographs are at a magnification of 250 diameters. Gross structural differences may readily be observed.

The specimen that exhibited smooth, parabolic weight change, shown in the left column of photomicrographs of figure 18, possesses what appears to be a single scale layer. The external surface of this scale (fig. 18(a)), is composed of a fine-grained oxide disposed on the alloy surface in an undulating pattern clearly seen in cross section (fig. 18(c)). The number and amplitude of these undulations, oriented perpendicular to the longest dimension of the specimen, indicate that they cannot arise as a result of differential thermal contraction. X-ray diffraction analysis of this scale indicated that it was composed basically of chromia admixed with some of the high-lattice-parameter spinel. Removal of the external scale, by light brushing, revealed metallic grains and intergranular oxidation (fig. 18(b)).

Photomicrographs of the specimen that exhibited an anomalous, large weight increment are shown on the right side of figure 18. The external scale is composed of several layers. The outermost zone consists of relatively large, faceted crystals identified by X-ray diffraction as cobalt monoxide; its surface topography is shown in figure 18(d). Within this compound outer zone is entrapped a continuous, thin, undulating layer which was identified as the low lattice parameter spinel (fig. 18(f)). Beneath the outer zone of the scale are two planar layers. The outer surface of the outer layer of this zone is shown (fig. 18(e)). Although the sequence of these two underlayers that comprise this zone is not known with certainty, both the X-ray diffraction and the X-ray fluorescence data indicate that the outermost one is cobaltous tungstate ($CoWO_4$) and that the one nearest the metal-oxide interface is a spinel. Metallographic evidence also suggests this layer sequence (fig. 18(f)).

Cross sections of these two scales are shown at a higher magnification in figure 19. A comparison of the photomicrographs illustrates that the morphology of the entrapped layer found in the coupon exhibiting high weight gain (fig. 19(b)) is nearly identical to that of the single-scale layer present on the coupon that exhibited low weight gain (fig. 19(a)). This observation strongly suggests that an undulating layer of chromia existed prior to the anomalous weight increment and that it was later infiltrated by cobalt monoxide and converted in place to the spinel by a solid-state diffusion reaction. The presence of voids near the interfaces of the entrapped layer (voids that may be of the Smigelskas-Kirkendall type (ref. 11)) reinforce this concept of in-place transformation. Differences in optical properties, and therefore the probable differences in chemical constitution necessary to this postulated scaling sequence, were verified by examination of the undulating layers using polarized light microscopy. The single-scale layer was optically active, exhibiting

Smooth, parabolic oxidation

(a) External surface.

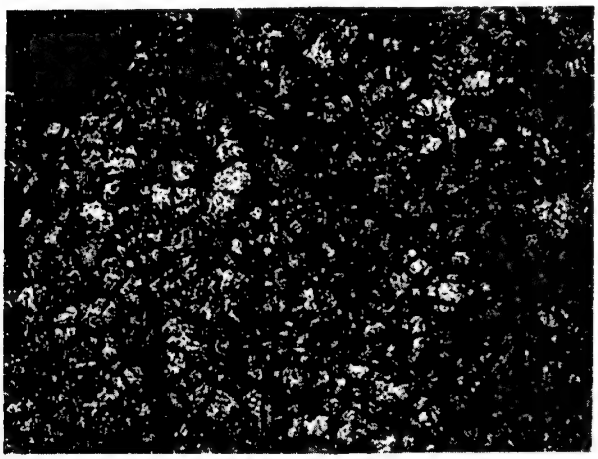

(b) First underlayer.

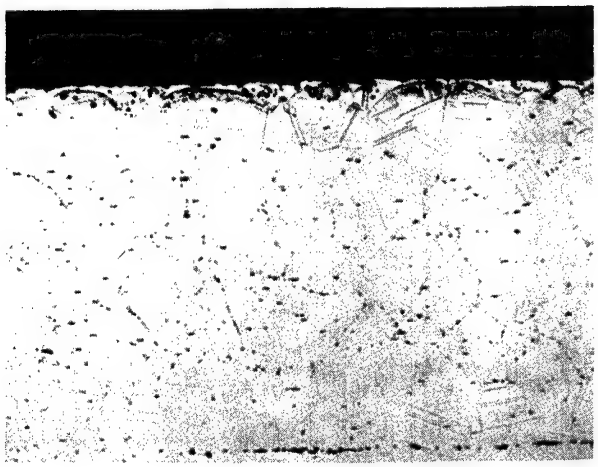

(c) Cross section.

Anomalous weight increment

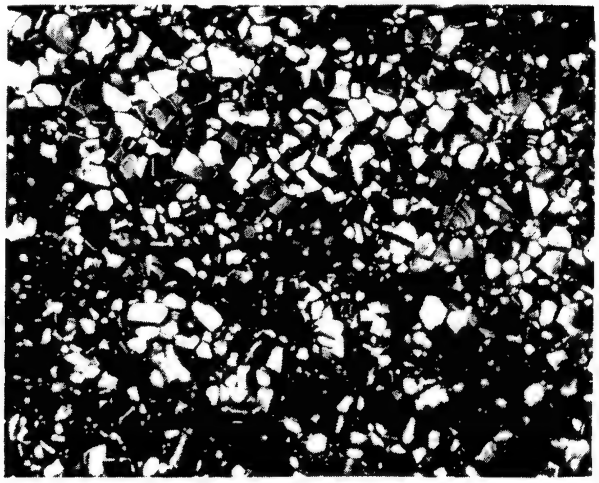

(d) External surface.

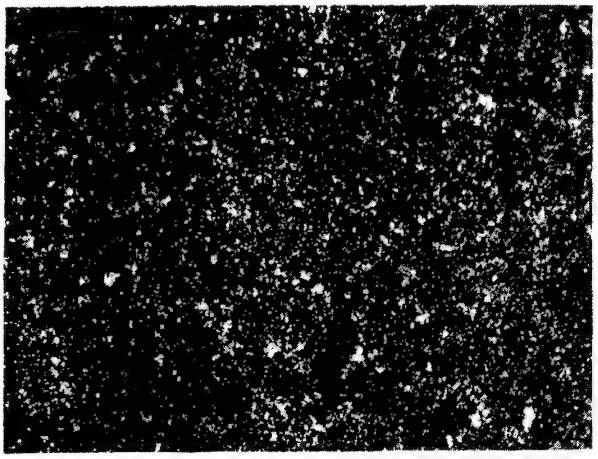

(e) First underlayer.

(f) Cross section.

Figure 18. - Structural character of specimens of heat 8 (0.12 wt % Si, 1.10 wt % Mn) oxidized in air for 4 hours at 1100° C. Etched in sulfuric acid - boric acid mixture. X250.

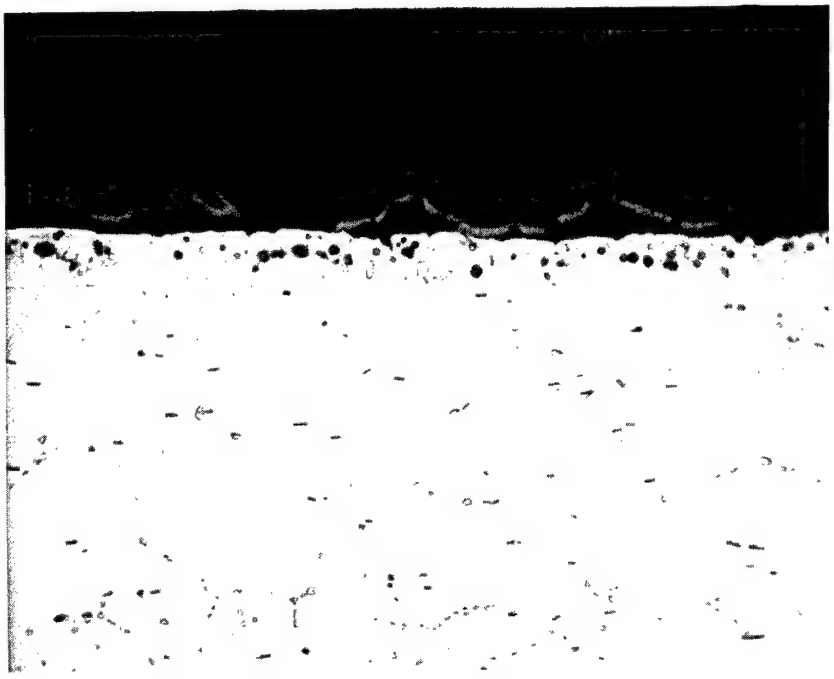

(a) Smooth, parabolic oxidation.

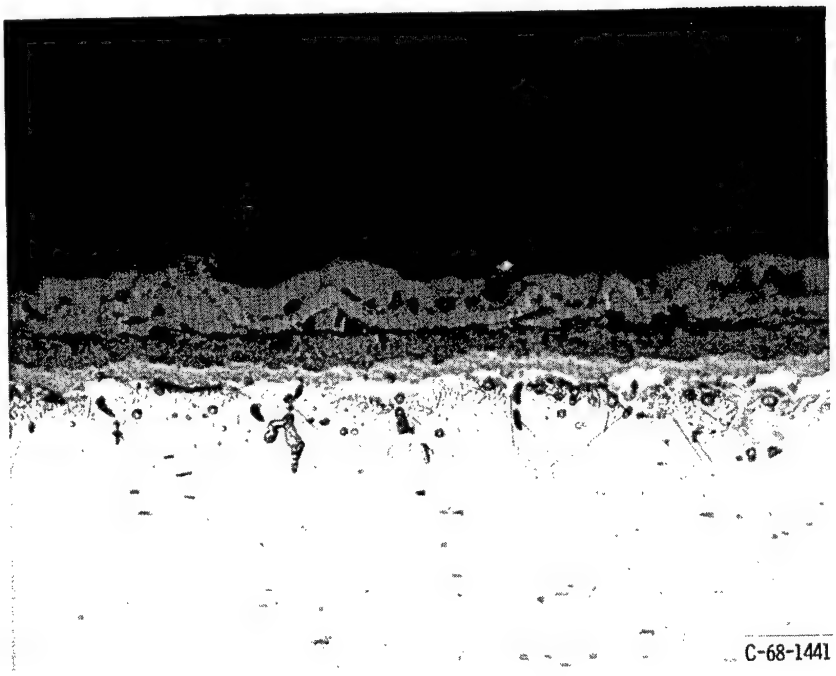

(b) Anomalous weight increment.

Figure 19. - Cross section of specimens of heat 8 (0.12 wt % Si, 1.10 wt % Mn) oxidized in air for 4 hours at 1100° C. Note undulating oxide layers. Etched in sulfuric acid - boric acid mixture. X500.

the green color characteristic of chromia, but the entrapped undulating layer was optically inactive as would be expected of a spinel phase.

X-ray fluorescence was employed to further explore the differences between these two specimens. In these determinations, the emitted intensity arising from excitation of each element within a specific geometric area is divided by the intensity arising from excitation of the same element in the unoxidized alloy. The resulting ratios are a qualitative measure of the concentration and distribution of elements in oxidized specimens. These data, for the two specimens under consideration, are presented in figure 20.

Results from the specimen that oxidized parabolically (low weight gain plots in fig. 20) indicate that the single-layered external scale is rich in both chromium and manganese. This is as expected because the scale was determined to be constituted of chromia and a high lattice parameter, manganese-rich spinel. The indicated tungsten concentration of the scale is believed to be too high and probably arises because of the transparency of the scale layer; that is, tungsten-rich material beneath the scale is excited, and, as a result, characteristic tungsten radiation passes through the scale and is detected. The alloy just beneath the scale (termed depletion zone) contains a strongly reduced chromium content and is almost totally depleted of manganese. This must qualitatively be so if these elements are consumed in the scaling reaction. Conversely, the alloy must be enriched in tungsten (fig. 20) if this element is not consumed in the external scale or otherwise lost to the specimen.

X-ray fluorescence results for the second specimen, which, during oxidation exhibited an anomalous weight increment, are also shown in figure 20 (high weight-gain curves). In this case, it was possible to obtain results representative of both an outer and an inner scale zone. This was facilitated by fracture of the scale along the nearly continuous void space shown in figure 19(b). Thus, the outer zone is constituted of cobalt monoxide and the entrapped, undulating spinel, whereas the inner zone is constituted of the two remaining planar scale layers.

The outer-scale zone is rich in manganese, which is most probably present as an oxide solid solution in cobalt monoxide although some of it may also be situated in the spinel phase. Chromium, also present, is probably somewhat richer than shown because the spinel with which it is associated is overlaid with cobalt monoxide which tends to shield the fluorescent chromium radiation. Tungsten, which nominally cannot react as part of either the spinel or the monoxide, is strongly deficient in the outer zone as expected.

The inner zone of the scale is moderately enriched with respect to both chromium and manganese and is strongly enriched with respect to tungsten. These results are in accord with the idea that the cobaltous tungstate layer overlies a spinel rich in both manganese and chromium.

As in the case of the high weight-gain specimen, both manganese and chromium are

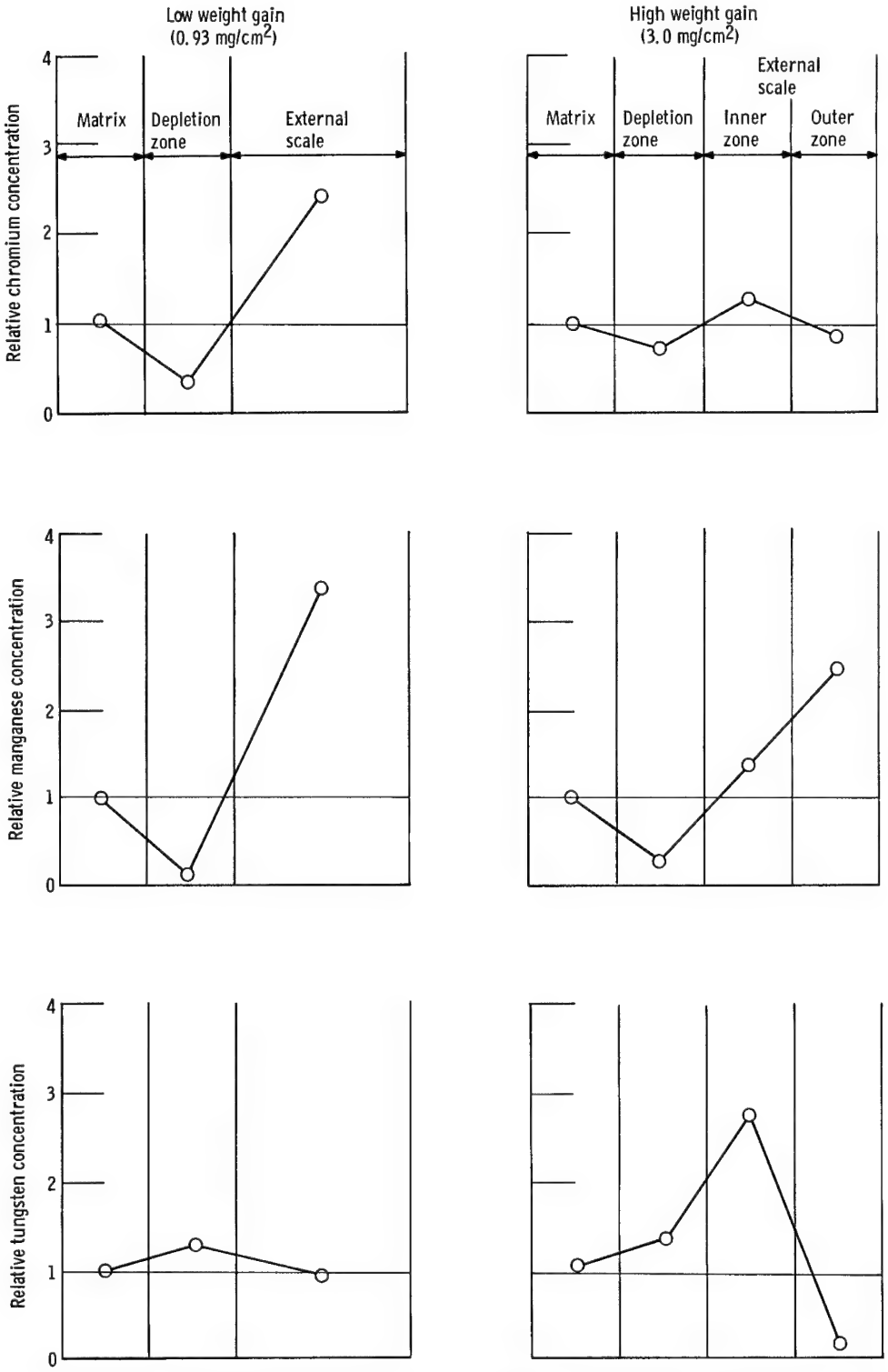

Figure 20. - Fluorescent analyses for chromium, manganese, and tungsten for various layers of specimens from heat 8 (0.12 wt % Si, 1.10 wt % Mn) oxidized in air for 4 hours at 1100° C. Specimens that exhibited smooth, parabolic oxidation (low ΔW) and an anomalous weight increment (high ΔW) are both shown.

depleted in the zone just beneath the scale layers, though the degree of depletion is not as strong. Tungsten is enriched in this zone, as before, in spite of the fact that is was consumed in the formation of the scale. This effect is believed to arise because the tungstate-forming reaction was both started and stopped during the overall scaling process. On initiation of a second spinel-producing reaction the observed enrichment of tungsten could occur both by diffusion of tungsten to the metal surface and by depletion of the other more reactive elements, especially manganese and chromium.

The X-ray fluorescence technique was also applied to a pair of specimens of the same heat oxidized for 100 hours at 1000° C. Although continuous weight-gain information was not obtained for this pair of nominally identical specimens, they exhibited a large difference in final weight gain (1.2 against 8.9 mg/cm^2). The fluorescence data for these two specimens (fig. 21) is nearly identical to that obtained for the analogous pair oxidized at 1100° C. These data imply that the scaling regime at 1000° C is quite similar to that at 1100° C and, further, implies that the inordinately large weight gains for this heat (fig. 4) probably arise from a single anomalous weight increment as was the case for the coupons oxidized at 1100° C. The strong similarity in these two independent sets of fluorescence data also reflects the degree of reproducability inherent with this technique.

These tests also indicated no large variations in iron concentration from one sampling position to the next, that is, from the scale to the depletion zone to the unoxidized matrix. This observation, coupled with the apparent independence of weight gain on iron concentration (fig. 11), strongly suggests that iron did not play a major role in the oxidation of L-605 at either 1000° or 1100° C.

Proposed scaling mechanism. - It has been demonstrated that the scaling of L-605 is a complex process dependent on temperature, time, and minor element concentration. In this section the chronology of the scaling of L-605 by a mechanism which is compatible with the above observations is qualitatively described. This will be done by considering those alloys that contain the lowest concentrations of silicon and manganese (0.12 wt % Si and 1.10 wt % Mn).

It is proposed that the oxidation reaction is initiated by the formation of an external scale of chromia which is nucleated and then grows laterally until a continuous film of chromium oxide (Cr_2O_3) is developed upon the alloy surface (fig. 22(a)). This film subsequently thickens by diffusional growth and thereby depletes the underlying alloy of chromium (see fig. 22(b)). During this stage of parabolic growth, a biaxial compressive stress (parallel to the alloy-oxide interface) is believed to be developed within the scale which tends to increase the interfacial area of the oxide with respect to that of the metal. A mechanism for the lateral growth of scales by deposition of material in oxide grain boundaries has been suggested previously (ref. 12).

The compressive stress must ultimately be relieved by plastic deformation of either the metal or the oxide, or both. Oxidation of a fine wire (approximately 0.25-mm diam)

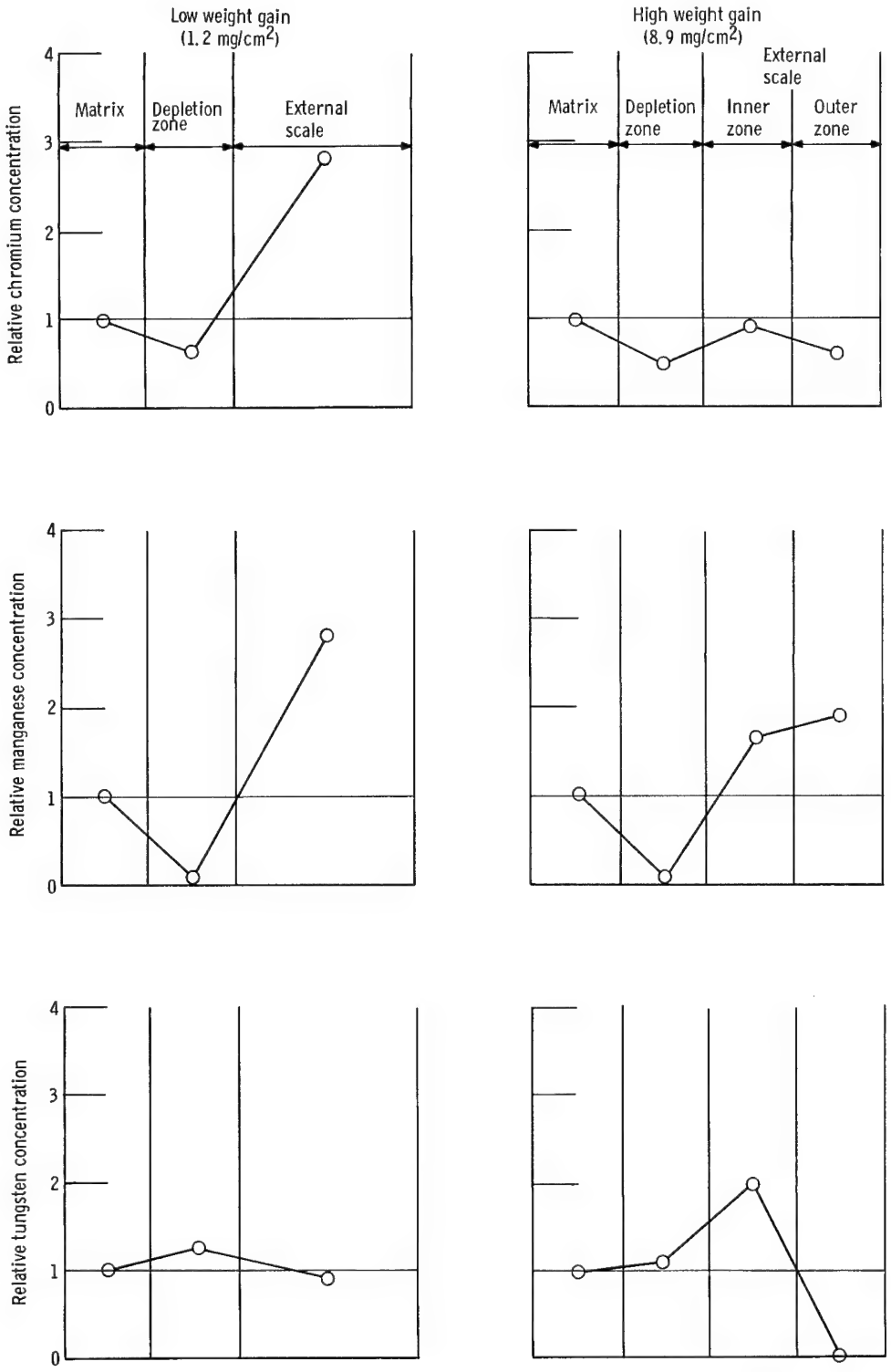

Figure 21. - Fluorescent analyses for chromium, manganese and tungsten for various layers of specimens from heat 8 (0.12 wt % Si, 1.10 wt % Mn) oxidized in air for 100 hours at 1000° C. Note similarities with corresponding analyses made for specimens oxidized at 1100° C (fig. 20).

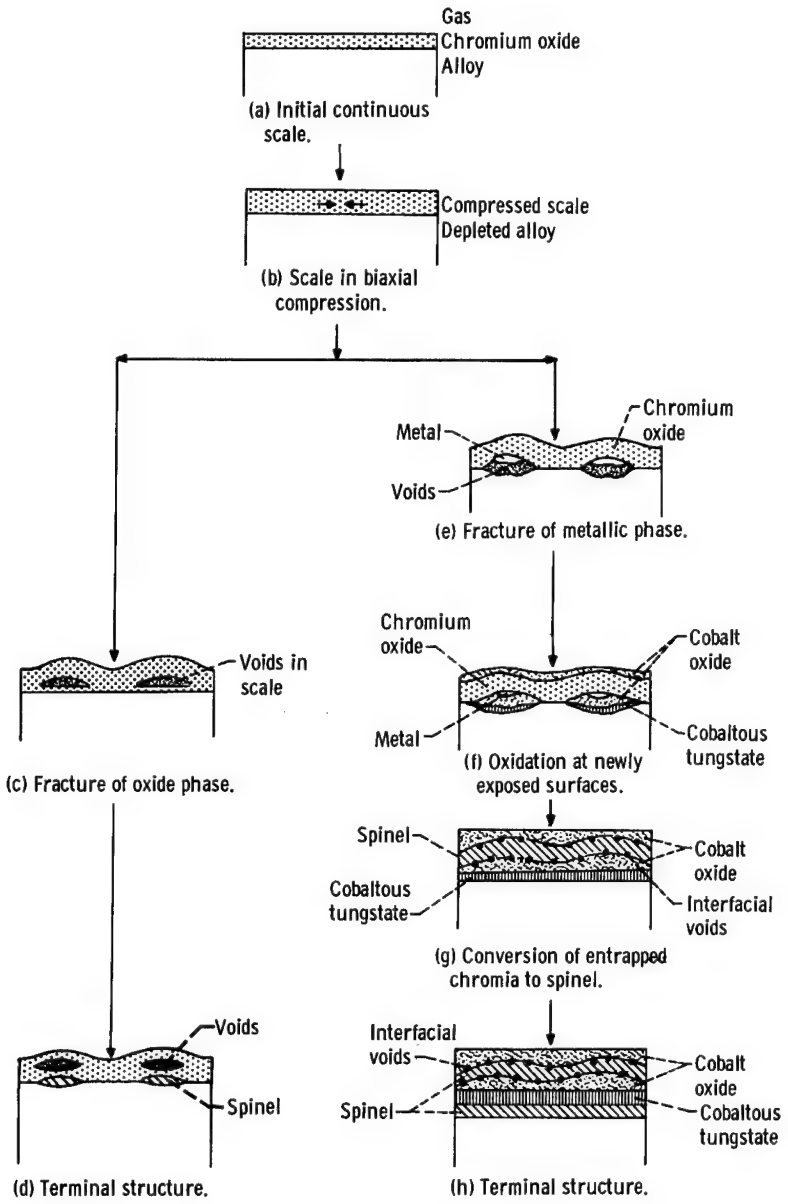

Figure 22. - Schematic representation of course of oxidation of L-605 showing two possible stress-relief modes. Center and left column - oxide fracture associated with smooth, nearly parabolic scale growth; center and right column - alloy fracture associated with anomalous weight increment.

of aged L-605 at 1000° C for 100 hours indicated that no appreciable axial growth of the bulk alloy occurred, probably because of the recognized superior elevated-temperature strength of this alloy. This observation suggests that deformation is restricted to a region close to the alloy-oxide interface and occurs either in the scale or in the weakened, depleted zone of the alloy.

It is postulated that the requisite plastic deformation leads to one of two distinct modes of failure. The first involves a relaxation of compressive scale stress by deformations that cause failure within the oxide phase (fig. 22(c)). This process produces an undulated scale layer of chromia (figs. 18(a) and (c) and 19(a)) which continues to grow by metal diffusion at points of contact between alloy and scale and ceases to increase in thickness at those points of the scale remote from the alloy. The remote portions of the scale become more porous to oxygen, principally by thermal faceting of the grain boundary network of the oxide, and this allows growth of oxide beneath the large void spaces of the scale to continue. The overall oxidation process, when integrated throughout the reaction surfaces, thus remains nearly parabolic in character. Finally, that portion of the chromia scale nearest the alloy reacts with its substrate, which is now enriched with relatively reactive manganese, to produce the high-lattice-parameter spinel (see fig. 22(d)). The foregoing mode of stress relaxation by failure of the scale thus leads to the continued parabolic scaling behavior observed in certain instances (see curve for heat 4, fig. 5).

The second possible stress relaxation process involves plastic deformation of the metallic phase of the specimen, ultimately leading to its failure. That the oxide possesses sufficient strength to provide this type of failure is suggested by the photomicrograph of figure 23. If the stressed oxide (fig. 22(b)) so disrupts the metal, then it is apparent that the area available to the oxidation reaction is greatly increased with respect to the assumed geometric reaction area (see fig. 22(e)). It is this process that is believed to be the origin of the observed anomalous weight increments.

This concept of increasing the reaction area and its direct consequences agree qualitatively with the sharpness, amplitude, and time dependence of the amplitude of the anomalous weight increments (fig. 15). It also accounts for details of the weight-gain-curve shape such as the later parabolic stage of oxidation and the accelerated rate just prior to this stage (fig. 17). The proposed areal increase is therefore, we believe, a more accurate physical description of the oxidation process than are earlier models for similar alloys (refs. 13 and 14) in which the weight increment is attributed to the oxidation of a chromium depleted zone just beneath the metal-oxide interface. Although this depleted zone probably plays some role in the weight-gain-acceleration process, it alone cannot be used to explain the observations concerning scale structure and weight-gain-curve shape made during the course of this research.

Once the anomalous increment has occurred, the process regains its parabolic character (fig. 17) and the scale develops to produce the structure shown in figure 19(b).

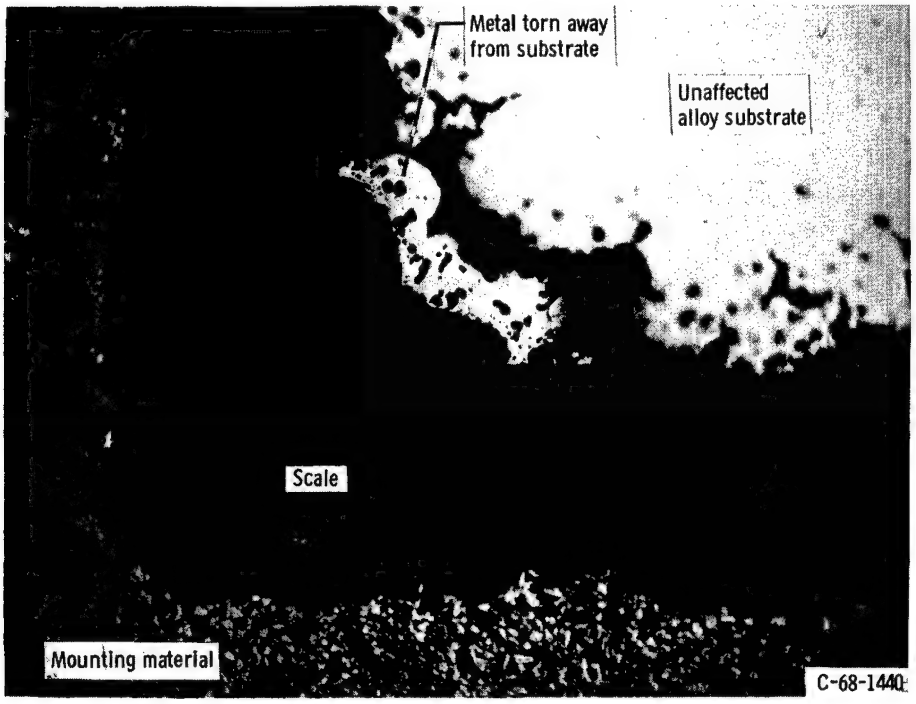

Figure 23. - Photomicrograph of corner of specimen of heat 8 (0.12 wt % Si, 1.10 wt % Mn) oxidized in air for 100 hours at 1100° C. Note tearing of metallic phase. Etched in sulfuric acid - boric acid mixture. X250.

Because the undulated chromia has been postulated to be porous to oxygen, and because the newly exposed surfaces are rich in cobalt and tungsten, a reaction ensues which produces both cobalt monoxide and cobaltous tungstate. Some cobalt is believed to diffuse through the nongrowing portions of the chromia layer to form cobalt monoxide at the outermost surface. Cobalt monoxide is also believed to form beneath this layer (fig. 22(f)). As a result, the undulated chromia is trapped within a cobaltous monoxide layer and converted in place to the undulated spinel layer (fig. 19(b)). The cobaltous tungstate, once nucleated, may continue to grow as a planar layer until such time as the tungsten is depleted and thereby separates the outer-scale layers from the alloy (see fig. 22(g)). Oxygen is subsequently supplied by or through the tungstate to the underlying alloy, strongly depleted in tungsten and somewhat depleted in chromium, and there reacts to nucleate and grow a second planar layer of spinel phase beneath the tungstate (figs. 19(b) and 22(h)). The occasional detection of unalloyed tungsten in or near the scale zone (table II) suggests that the cobaltous tungstate may, in fact, decompose to provide the oxygen for this reaction.

X-ray fluorescence and weight-gain data suggest that this general mechanism may apply equally well at both 1000° and 1100° C. The lack of experimental evidence presently precludes its application to the 1200° C oxidation tests. It is also possible that this

mechanism can explain similar anomalous weight increments observed during the scaling of other alloys. For example, in the high-temperature oxidation of stainless steel, weight-gain curves like those shown in figure 15 were obtained (ref. 15). In addition, a similar behavior has been observed for nickel-chromium, cobalt-chromium, and other iron-chromium alloys (refs. 13 and 14). We believe that the preceeding description of the anomalous weight-gain phenomena may also be extended to alloys that do not contain chromium, provided that the oxidation process produces a strong, highly-stressed oxide layer on a relatively weak metallic substrate.

The specific process which we have proposed for the anomalous weight gain is, of course, not required to describe the oxidation of L-605 alloy heats outside of the unstable region (as defined by the combined concentrations of silicon and manganese). The reasons for this gross change in behavior with relatively minor changes in alloy chemistry is presently unclear. There are, however, a few possible phenomena that might be considered:

(1) Relatively high manganese concentrations may promote the formation of manganese-bearing scale phases that weaken the scale and allow it to absorb the strain due to growth stresses. This would, in turn, preclude fracture through the metallic phase and the accompanying weight increment.

(2) Higher silicon concentrations will promote Laves phase formation (ref. 4), especially in the region of alloy grain boundaries. Subsequent internal oxidation of this phase, with appropriately directed diffusion fluxes, may produce a lateral dilatation of the metal surface. If produced, this dilatation would counteract a portion of the tensile stress in the metal, imposed by the external scale, and reduce the tendency for metal tearing.

(3) Manganese or silicon may act in a catalytic manner to change the chemical nature and/or the oxide microstructure in the scale layer thereby reducing its potential for stress generation and for subsequent fracture of the alloy.

SUMMARY OF RESULTS

An investigation was conducted to determine the effect of silicon concentration on the oxidation behavior of the cobalt-base superalloy L-605. Seven heats of this alloy, varying in composition but within the Aerospace Materials Specification ranges for chemical composition, were oxidized in air at 1000°, 1100°, and 1200° C for times up to 225 hours. The oxidation processes were monitored by intermittent and continuous weight-gain measurements, by X-ray diffraction and fluorescent analyses, and by metallographic analyses. A mechanism describing the course of oxidation was postulated which may be extended to other classes of alloys. The following results were obtained:

1. Compositional plots, developed for each temperature of oxidation, indicated that

the oxidation resistance of L-605 could be optimized with respect to alloy composition. Available post-aging ductility data for L-605, when plotted in the same way, exhibited a high-ductility region different from that for optimum oxidation resistance. The two regions did, however, exhibit a compositional area of overlap which represents simultaneous optimization of both oxidation resistance and post-aging ductility. From this, it is inferred that only those alloys containing 0.1- to 0.4-weight-percent silicon with 1.4- to 1.65-weight-percent manganese be utilized as high-temperature, oxidation-resistant, load-bearing materials.

2. Alloy heats within this optimum composition range oxidized in a smooth, nearly parabolic fashion, and the scales were found to be rich in chromia and a high-lattice-parameter spinel, which probably contained manganese.

3. Alloy heats outside the optimum oxidation composition range oxidized more rapidly and in an unpredictible fashion, often exhibiting large, anomalous weight gains. Scales of a complex nature with respect to both structure and chemistry were developed in these instances.

Lewis Research Center,
National Aeronautics and Space Administration,
Cleveland, Ohio, April 22, 1968,
129-03-01-04-22.

REFERENCES

1. Jenkins, E. E.: Embrittlement of Haynes Alloy No. 25 During Brazing. Rep. No. 817-1390, Haynes Stellite Co., May 21, 1958.

2. Evans, E. B.; Vargo, E. J.; and Pearson, J. B.: Embittlement of Haynes Alloy No. 25 (L-605) During High Temperature Exposure. Rep. TM-3488, TRW Inc., Aug. 17, 1962.

3. Wlodek, S. T.: Embrittlement of a Co-Cr-W (L-605) Alloy. Trans. ASM, vol. 56, no. 3, Sept. 1963, pp. 287-303.

4. Sandrock, Gary D.; Ashbrook, Richard L.; and Freche, John C.: Effect of Variations in Silicon and Iron Content on Embrittlement of a Cobalt-Base Alloy (L-605). NASA TN D-2989, 1965.

5. Nejedlik, J. F.: The Embrittlement Characteristics of a Low-Silicon Modified Cobalt-Base Alloy (L-605) at 1200° and 1600° F. Rep. ER-6870, TRW Inc., June 15, 1966.

6. Sandrock, Gary D.; and Leonard, L.: Cold Reduction as a Means of Reducing Embrittlement of a Cobalt-Base Alloy (L-605). NASA TN D-3528, 1966.

7. Wlodek, S. T.: The Oxidation of L-605 and X-40. Rep. R64FPD12, General Electric Co., Jan. 24, 1964.

8. Charlot, L. A.; and Westerman, R. E.: High Temperature Corrosion and Evaporation of Haynes 25 and Hastelloy X-280. Corrosion, vol. 23, no. 2, Feb. 1967, pp. 50-56.

9. Bardos, D. I.; Gupta, K. P.; and Beck, Paul A.: Ternary Laves Phases with Transition Elements and Silicon. Trans. AIME, vol. 221, no. 5, Oct. 1961, pp. 1087-1088.

10. Rhines, Frederick N.: Phase Diagrams in Metallurgy. McGraw-Hill Book Co., Inc., 1956, pp. 125-175.

11. Smigelskas, A. D.; and Kirkendall, E. O.: Zinc Diffusion in Alpha Brass. Trans. AIME, vol. 171, 1947, pp. 130-135.

12. Wolf, James S.: An Investigation of the Effect of Specimen Geometry on the Oxidation of Nickel at Elevated Temperatures. PhD Thesis, Univ. Florida, 1965.

13. McCullough, H. M.; Fontana, M. G.; and Beck, F. H.: Formation of Oxides on Some Stainless Steels at High Temperatures. Trans. ASM, vol. 43, 1951, pp. 404-420.

14. Davin, A.; Coutsouradis, D.; and Habraken, L.: Dry Corrosion of Cobalt-Chromium Alloys at High Temperature - Influence of Ternary Additions. Cobalt, no. 35, June 1967, pp. 69-77.

15. Bénard, Jacques; Hertz, Jean; Jeanin, Yves; and Moreau, Jean: Sur le mecanisme d'oxydation aux températures élevées de l'acier austénitique 18 % Cr - 8 % Ni. Acad. Sci. Comp. Rend., vol. 248, Apr. 6, 1959, pp. 2095-2097.

NASA-Langley, 1968 —— 17 E-4378

"The aeronautical and space activities of the United States shall be conducted so as to contribute . . . to the expansion of human knowledge of phenomena in the atmosphere and space. The Administration shall provide for the widest practicable and appropriate dissemination of information concerning its activities and the results thereof."

—NATIONAL AERONAUTICS AND SPACE ACT OF 1958

NASA SCIENTIFIC AND TECHNICAL PUBLICATIONS

TECHNICAL REPORTS: Scientific and technical information considered important, complete, and a lasting contribution to existing knowledge.

TECHNICAL NOTES: Information less broad in scope but nevertheless of importance as a contribution to existing knowledge.

TECHNICAL MEMORANDUMS: Information receiving limited distribution because of preliminary data, security classification, or other reasons.

CONTRACTOR REPORTS: Scientific and technical information generated under a NASA contract or grant and considered an important contribution to existing knowledge.

TECHNICAL TRANSLATIONS: Information published in a foreign language considered to merit NASA distribution in English.

SPECIAL PUBLICATIONS: Information derived from or of value to NASA activities. Publications include conference proceedings, monographs, data compilations, handbooks, sourcebooks, and special bibliographies.

TECHNOLOGY UTILIZATION PUBLICATIONS: Information on technology used by NASA that may be of particular interest in commercial and other non-aerospace applications. Publications include Tech Briefs, Technology Utilization Reports and Notes, and Technology Surveys.

Details on the availability of these publications may be obtained from:

SCIENTIFIC AND TECHNICAL INFORMATION DIVISION

NATIONAL AERONAUTICS AND SPACE ADMINISTRATION

Washington, D.C. 20546